Mathematical Modelling and Numerical Simulation with Applications, 2024, 4(1), 1–36

https://dergipark.org.tr/en/pub/mmnsa
ISSN Online: 2791-8564 / Open Access
https://doi.org/10.53391/mmnsa.1373093

RESEARCH PAPER

Mathematical approaches to controlling COVID-19: optimal control and financial benefits

Saida Id Ouaziz [1,*,‡] and **Mohammed El Khomssi** [1,‡]

[1]Department of Mathematics, Laboratory of Modeling and Mathematical Structures, Sidi Mohamed Ben Abdellah University, Route d'Ilmouzzer, 30000 Fez, Morocco

*Corresponding Author
‡ saidaidouaziz7@gmail.com (Saida Id Ouaziz); khomsixmath@yahoo.fr (Mohammed El Khomssi)

Abstract

The global population has suffered extensively as an effect of the coronavirus infection, with the loss of many lives, adverse financial consequences, and increased impoverishment. In this paper, we propose an example of the non-linear mathematical modeling of the COVID-19 phenomenon. Using the fixed point theorem, we established the solution's existence and unicity. We demonstrate how, under the framework, the basic reproduction number can be redefined. The different equilibria of the model are identified, and their stability analyses are carefully examined. According to our argument, it is illustrated that there is a single optimal control that can be used to reduce the expense of the illness load and applied processes. The determination of optimal strategies is examined with the aid of Pontryagin's maximum principle. To support the analytical results, we perform comprehensive digital simulations using the Runge-Kutta 4th-order. The data simulated suggest that the effects of the recommended controls significantly impact the incidence of the disease, in contrast to the absence of control cases. Further, we calculate the incremental cost-effectiveness ratio to assess the cost and benefits of each potential combination of the two control measures. The findings indicate that public attention, personal hygiene practices, and isolating oneself will all contribute to slowing the spread of COVID-19. Furthermore, those who are infected can readily decrease their virus to become virtually non-detectable with treatment consent.

Keywords: Cost-effectiveness; optimal control; system dynamics

AMS 2020 Classification: 34D20; 92D30; 49J15; 34C60

1 Introduction

The world is facing an unprecedented threat. The pandemic of COVID-19 has spread rapidly throughout the worldwide community. As a result of this epidemic, suffering has spread, the lives of billions of people have turned upside down, and the global economy is under threat. Even

➤ **Received:** 09.10.2023 ➤ **Revised:** 02.01.2024 ➤ **Accepted:** 21.01.2024 ➤ **Published:** 31.03.2024

wealthy countries with robust healthcare systems are under pressure as the wave of this pandemic begins to reach countries already suffering humanitarian crises from conflicts, natural disasters, and climate change.

The first instance of a virus whose etiology is completely unexplained was identified in the Chinese, on December 31, 2019 [1]. Moreover, this pandemic demands immediate and sustained international action. While reducing the scale of the terrible human and economic toll across the globe is our primary concern, we are also very concerned about the underlying problems that this emergency reveals, particularly for those most at risk of disastrous consequences. This group of viruses called coronaviruses is responsible for gastrointestinal and respiratory illnesses in many different world locations. Both the common cold and more severe illnesses can be respiratory disorders. Since they resemble coronas under the microscope, coronaviruses received their name. An infused envelope surrounds the genetic material center of the virus. It resembles a crown as a result of this. In Latin, the corona is a word that signifies "crown". Most people infected with the virus have minor or moderate lung disease and recover without seeking treatment. Some, however, get severe illnesses and need to see a doctor. Seniors and patients with prior illnesses such as cancer, glucose intolerance, permanent lung illness, or heart disease are more prone to have a severe variation. The most effective strategy to avoid and limit transmission of COVID-19 is to be knowledgeable about the illness and how it is spread. Anyone, at any age, can contract the illness and become extremely ill or die from it.

The World Health Organization (WHO) has designated the 2019 coronavirus disease (COVID-19) as a global epidemic. To stop the virus from spreading further, a concerted international effort is required. "Occurring over a huge geographic area and impacting an extraordinarily high proportion of the population" is how a pandemic is described. The H1N1 flu pandemic in 2009 was the most recent pandemic to be reported globally. Mathematical models hold significance as they elucidate the fundamental mathematical structure of a specific phenomenon without delving into extraneous details. The purpose is to concentrate on certain facets of the issue, abstracting away other dimensions. Consequently, mathematical models remain pertinent by showcasing the essential mathematical core within a given context devoid of excess information [2] (see also [3], [4], [5] and reference therein).

To reduce the COVID-19 disease's transmission dynamics, the authors of [6] studied and discussed an optimal control model. The limitations of the illness and the associated expenses are also minimized by suggesting the most appropriate control measures. They established its existence and specificity. Further data simulations are performed to observe the importance of control efforts to stop the propagation of the illness in society according to a study that was done on the spread of disease between countries based on an estimated COVID-19 mathematical model. The study in [7] explores a mathematical model that involves the effects of resource constraints on COVID-19 transmission patterns in the population through the use of the Caputo derivative. The basic reproduction rate R_0 was determined, and the suggested model's asymptotic stability was investigated. According to their findings, the number of people with the virus increases, while cure rates by hospitalization increase. The authors of [8] analyze the dynamics of a fractional-order COVID-19 model and suggest an efficient computational technique based on the domain discretization and memory concept to numerically solve this fractional-order corona model The coronavirus is an enclosed virus with a single-stranded, positive-sense RNA that is a component of the Nidovirales demand and the relative Coronaviridae. It is widely transmitted among mammals and humans [9]. To understand COVID-19's effects on the environment, the authors suggest mathematical modeling and data analysis in [10]. Such a pandemic is mathematically modeled as a deterministic infectious illness. They use the fixed-point theorem to confirm the originality of the solution, and it is inferred that the sample displays both endemic and disease-free equilibrium points. Further,

they propose an optimal control to find the best strategy to eliminate the virus.
With the Atangana-Baleanu derivative, [11] provides a rigorous mathematical analysis of the intricacies of smoking behavior and its public health implications. The authors in [12] propose and analyze a compartmental deterministic framework to explain the behavior of the student population's illicit drug usage. The bifurcation phenomenon is identified using the Center Manifold Theorem. Efficiency analysis is applied to understand how the dynamics of illicit drug use by the student group are influenced by the settings of the system. Assessing the epidemiology of the patients, the clinical course of the condition, and the available treatment options, Tang et al. created a model [13]. A sensitivity analysis suggests that actions regarding isolation and quarantine can lower it. Numerous mathematical model types use statistical techniques to research the COVID-19 virus (see, for example, [14]).
The authors of [15] Create a compartmental model to evaluate the effects of mask use on the population as a whole among the general, asymptomatic public, some of whom may be asymptomatically infected. They imply that the public's adoption of face masks has a strong potential for reducing the spread of the pandemic and its burden. The study in [16] examines the affordability and effectiveness of three malaria-prevention measures. They found that one of the conclusions was that treating infected people and spraying insecticides was the most cost-effective way of eliminating malaria. The authors of [17] treat three disease compartments: infectious, quarantined, and exposed-asymptomatic, and they indicate that the rate of treatment is a saturated type to account for the impact of scarce medical facilities. By taking into account the implications on infection transmission rates caused by the adoption of lockdown policies by numerous countries, they also developed an optimal control issue. In [18], a decision analytical model of different cases of ratios of people without symptoms of COVID-19 and dangerous intervals predicts propagation from untreated persons for more than half of all transmissions. Thus, the virus mitigation measures that can halt the disease's circulation must receive resources and health information.
The literature contains several mathematical models that explain how COVID-19 propagates and recommend measures to optimize virus transmission. The authors in [19] observed that, in the absence of immunization, using either physical distancing or social separation procedures is the most economical and successful management approach in Saudi Arabia. In [20], a study introduces a mathematical framework for monitoring and predicting the spread of COVID-19 in India, using data up to April 30, 2020. The authors calculate the ratio R_0 and perform local and global stability analyses. The template expects a significant spread with a peak after almost 60 days, implying the persistence of the illness even after reaching a certain level. The study in [21] presents a new mathematical model to analyze the omicron variant of COVID-19, exploring stability conditions and extensions. Using realistic data from South Africa, numerical simulations highlight the effectiveness of WHO recommendations in reducing infection. Investigations on the transmission of COVID-19 and epidemic patterns concentrate on sample selection and adequate control measures. The essay [22] reviews mathematical models, highlighting the importance of reasonable parameter control and combined multi-model modeling for future interventions. The previously mentioned literature serves as an inspiration for our work's motivation and originality. In our case, we have adopted this model as the most realistic example as it deals with the predominant classes in society for this virus by presenting declared and undeclared infections, as well as contributing to a more thorough comprehension of the course of the disease and enabling Morocco to modify its disorder treatment tactics.
The structure of this essay is as detailed below: In Section 2, we present some theorems used in this essay. The mathematical model is developed in Section 3. In Section 4, the well-established nature of the system is examined. The ratio $\mathcal{R}_0$ is given, as are the local and global stability of the equilibrium points. Section 5 illustrates the importance of every model factor concerning

$\mathcal{R}_0$. In Section 6, an analysis of an optimal control model is provided. Data of simulation and verification are given in Section 7, while, Section 8 is dedicated to the model's cost-effectiveness analysis. Eventually, Section 9 summarizes the current work.

2 Fundamental prerequisites

The upcoming sections of the paper will utilize the following theorems:

The following theorems (see [23, 24]), whose proofs will be given in the later sections, will be used to discuss the constancy of the template's steadiness point:

Theorem 3
If $\mathcal{R}_0 < 1$, the point of disease-free equilibrium DFE is locally asymptotically stable; nevertheless, if $\mathcal{R}_0 > 1$, it is unstable.

Theorem 4
If $\mathcal{R}_0 < 1$, the DFE, $\mathcal{E}_0$ of model (2), is globally equilibrium-stable.

Theorem 6
Where $\mathcal{R}_0 > 1$, the persistent steadiness point $\tilde{\mathcal{E}}$ is locally asymptotically stable.

Theorem 7
The only persistent steadiness state of (2) is globally asymptotically stable when $\mathcal{R}_0 > 1$.

3 Description of the model

To establish a new deterministic model, we begin by analyzing crucial characteristics of the COVID-19 pandemic, such as the presence of individuals who evaluated positively for the virus but did not exhibit any indications of illness and the splitting of pathogenic categories into two crucial categories: Contaminated people and ill individuals who have not yet received an official diagnosis. The general community $N(t)$ is partitioned into six sub-populations: sensitive $\mathfrak{S}_I(t)$, unprotected $E_I(t)$, contaminated or exhibiting indications $I(t)$, those who are ill but are not yet officially diagnosed $\mathcal{I}_{nd}$ recuperated individuals $R(t)$ and healthy $H(t)$, Π is the recruitment number, μ is the natural mortality rate, μ_1 is the patient mortality due to human coronavirus infection. ν represents the rate of infection diffusion from E_I to $\mathfrak{S}_I$, and σ is the saturation constant, β stands for incidence rate, α indicates the percentage of people from the exposed compartment who join the diseased subpopulation, δ is the rate at which those who are exposed to an infection contract it, γ is the interaction between I_nd and R, while θ is the rate at which susceptible people become uninfected, η is the rate of recovered individuals from COVID-19, when the entire population grows to a level equivalent to $N = \mathfrak{S}_I + E_I + I + \mathcal{I}_{nd} + R + H$. Without estimating the number of pathogens present within each individual, models built on this type of construction merely represent the infected individuals' community attitude. Our model, based on an illustration depicting the biological mechanism of coronavirus in humans, is depicted in Figure 1.

To consistently explore a mathematical framework of a real-world phenomenon, it is vital to specify these criteria by indicating a set of conditions. We enumerate these conditions in the above section, as outlined in [25]:

(a) Depending on the prototype, an estimated intake of susceptible individuals costs Π per unit of time.

(b) It simply considers how the pandemic progresses among individuals.

(c) The framework provides for the natural death of each sub-population in proportion to its size. Although most studies indicate that all people are contaminated with the virus, it is not possible to exclude the minority who are not (the individuals H), which is due to immunity and lifestyle. The dynamics of infection in the human populace are represented by the following set of six distinct equations and can be formulated in the following manner:

$$\begin{cases} \frac{d\mathfrak{S}_I}{dt} &= \Pi - \nu\mathfrak{S}_I I - (\mu+\theta)\mathfrak{S}_I, \\ \frac{dE_I}{dt} &= \nu\mathfrak{S}_I I - \delta E_I - \mu E_I, \\ \frac{dI}{dt} &= \alpha\delta E_I - \eta I - (\mu+\mu_1)I, \\ \frac{d\mathcal{I}_{nd}}{dt} &= (1-\alpha)\delta E_I - \gamma\mathcal{I}_{nd} - (\mu+\mu_1)\mathcal{I}_{nd}, \\ \frac{dR}{dt} &= \eta I + \gamma\mathcal{I}_{nd} - \mu R, \\ \frac{dH}{dt} &= \theta\mathfrak{S}_I - \mu H, \end{cases} \tag{1}$$

with the initial condition: $\mathfrak{S}_I(0 \geq 0, E_I(0) \geq 0, I(0) \geq 0, \mathcal{I}_{nd}(0) \geq 0, R(0) \geq 0, H(0) \geq 0$.

- Characteristics of susceptible individuals:

The population recruits susceptible members $\mathfrak{S}_I$ at a constant rate, Π, and the natural mortality rate μ reduces their numbers, the population $\mathfrak{S}_I$ will join the subpopulation I passing through E_I at the rate ν, although some of these individuals will have contact with H at a steady rate θ.

- Characteristics of exposed people:

The rate at which the exposed person E_I declines is δ for asymptomatic people and μ for natural death. Individuals E_I and sensitive individuals $\mathfrak{S}_I$ shall immediately interact at a steady rate of ν, E_I gets sicker by a fixed percentage α at a rate δ, where part of this population is not declared as diseased $((1-\alpha)\delta)$.

- Characteristics of undeclared people:

Without a diagnosis, the classes $\mathcal{I}_{nd}$ are transferred to the recovery classes at the rate γ.

- Characteristics of healthy individual:

Sensitive individuals $\mathfrak{S}_I$ interact with individuals in the population that is immune and has never contracted the disease (H) at a θ rate.

- Characteristics of individuals with disease signs:

The unaffected people give birth to the affected people when the coronavirus clinical symptoms progress. A constant share α of the exposed people transitions to the affected classes at a rate of δ. the class I transferred at a rate of η to the recover classes.

- Characteristics of recuperated individuals:

It can be presumed that the population that has recovered has long-lasting protection against coronavirus. Individual $\mathcal{I}_{nd}$ and population I recover from the coronavirus at γ and η rates, respectively. The rate of recovery deaths is μ.

- Characteristics of healthy individuals:

According to a study by Imperial College London, people with a high quantity of T cells (white blood corpuscle that contributes to the organism's defense against infection) from the coronaviruses responsible for the common cold are less likely to contract SARS-CoV-2, the virus responsible for COVID-19. So we named these individuals 'healthy' H. Thus, the sensible population $\mathfrak{S}_I$ moved to the category H at a rate of θ. Table 1 lists the parameters and variables in detail.

Table 1. Model parameters and their meanings

Parameters	Description
$\mathfrak{S}_I(t)$	The portion of sensitive individuals who are in direct interaction with an infected individual.
$E_I(t)$	The portion of those revealed to I that does not maintain them out.
$I(t)$	The portion of those who are impacted.
$\mathcal{I}_{nd}(t)$	The portion of non-reported infected person.
$R(t)$	The portion of rescued people.
$H(t)$	The portion of strictly asymptomatic individuals who have never caught the infection.
Π	Recruitment number
μ	The rate of natural mortality
μ_1	Natural death rate of human coronavirus illness patients
ν	Rate of diffusion of infection from E_I to $\mathfrak{S}_I$
σ	The constant of saturation
β	Incidence rate
α	Percentage of people from the exposed compartment who eventually migrate to the sick subpopulation
δ	The rate of illness in exposed individuals
η	Rate of COVID-19 patients that have recovered
γ	The rate at which $\mathcal{I}_{nd}$ interacts with R
θ	The rate at which sensitive persons become uninfected

4 Qualitative analysis of the model

This section will investigate a few key aspects of the suggested model, including its boundary, the presence of a steady state, and the fundamental reproduction number.

The presence and singular nature of the solutions to the framework

With applying the fixed point theorem and the premises that $\mathcal{H} = (\mathfrak{C}(\mathfrak{J}))^6$, and $\mathfrak{C}(\mathfrak{J})$ remains a Banach domain for continuous functions along the interval $\mathfrak{J}$ during the norm

$$\|\mathfrak{g}_i(t)\|_{i=1,\ldots,6} = \sum_{i=1}^{6} \|\mathfrak{g}_i\|_\infty,$$

where, $(\mathfrak{g}_1, \mathfrak{g}_2, \mathfrak{g}_3, \mathfrak{g}_4, \mathfrak{g}_5, \mathfrak{g}_6) = (\mathfrak{S}_I, E_I, I, \mathcal{I}_{nd}, R, H)$.
It can be demonstrated that the configuration outlined (1) has a valid outcome. Here, $\|.\|_\infty$ represents the maximum norm in $\mathfrak{C}(\mathfrak{J})$.

For the sake of simplicity, let us examine:

$$\begin{aligned}
&\Theta_1(t,\mathfrak{S}_I) = \Pi - \nu\mathfrak{S}_I I - (\mu+\theta)\mathfrak{S}_I,\\
&\Theta_2(t,E_I) = \nu\mathfrak{S}_I I - \delta E_I - \mu E_I,\\
&\Theta_3(t,I) = \alpha\delta E_I - \eta I - (\mu+\mu_1)I,\\
&\Theta_4(t,\mathcal{I}_{nd}) = (1-\alpha)\delta E_I - \gamma\mathcal{I}_{nd} - (\mu+\mu_1)\mathcal{I}_{nd},\\
&\Theta_5(t,R) = \eta I + \gamma\mathcal{I}_{nd} - \mu R,\\
&\Theta_6(t,H) = \theta\mathfrak{S}_I - \mu H.
\end{aligned}$$

To prove this theorem, we suppose that
$\|\mathfrak{S}_I\| \leq \mathfrak{w}_1, \|E_I\| \leq \mathfrak{w}_2, \|I\| \leq \mathfrak{w}_3, \|\mathcal{I}_{nd}\| \leq \mathfrak{w}_4, \|R\| \leq \mathfrak{w}_5, \|H\| \leq \mathfrak{w}_6$ where $\mathfrak{w}_i, i = 1,...,6$ are constant positives. Hence, we denote

$$\begin{aligned}
&\mathfrak{k}_1 = \nu\mathfrak{w}_3 + \theta + \mu,\\
&\mathfrak{k}_2 = \alpha\delta + \delta + \mu,\\
&\mathfrak{k}_3 = \eta + \mu + \mu_1,\\
&\mathfrak{k}_4 = \gamma + \mu + \mu_1,\\
&\mathfrak{k}_5 = \mathfrak{k}_6 = \mu.
\end{aligned}$$

Theorem 1 *If the proposed inequality is true, the $\Theta_{i=1,...6}$ are adapted to the Lipschitz state and compaction.*

$$0 \leq \mathfrak{k}_{i=1,...,6} < 1.$$

Proof Consider the functions $\mathfrak{S}_{I_1}$ and $\mathfrak{S}_{I_2}$, so

$$\|\Theta_1(t,\mathfrak{S}_{I_1}) - \Theta_1(t,\mathfrak{S}_{I_2})\| = \|-(\nu I + \mu + \theta)(\mathfrak{S}_{I_1} - \mathfrak{S}_{I_2})\| \leq (\nu\mathfrak{w}_3 + \theta + \mu)\|\mathfrak{S}_{N_1}(t) - \mathfrak{S}_{N_2}(t)\|.$$

Thus

$$\|\Theta_1(t,\mathfrak{S}_{I_1}) - \Theta_1(t,\mathfrak{S}_{I_2})\| \leq \mathfrak{k}_1\|\mathfrak{S}_{I_1}(t) - \mathfrak{S}_{I_2}(t)\|.$$

The Lipschitz criterion is achieved for Θ_1. Similarly, the Lipschitz condition for Θ_2, Θ_3, Θ_4, Θ_5, and Θ_6 may be easily proven and is the same as stated previously:

$$\|\Theta_2(t,E_{I_1}) - \Theta_2(t,E_{I_2})\| \leq \mathfrak{k}_2\|E_{I_1}(t) - E_{I_2}(t)\|,$$

$$\|\Theta_3(t,I_1) - \Theta_3(t,I_2)\| \leq \mathfrak{k}_3\|I_1(t) - I_2(t)\|,$$

$$\|\Theta_4(t,U_{d_1}) - \Theta_4(t,U_{d_2})\| \leq \mathfrak{k}_4\|U_{d_1}(t) - U_{d_2}(t)\|,$$

$$\|\Theta_5(t,R_1) - \Theta_5(t,R_2)\| \leq \mathfrak{k}_5\|R_1(t) - R_2(t)\|,$$

$$\|\Theta_6(t, H_1) - \Theta_6(t, H_2)\| \leq \mathfrak{k}_6 \|H_1(t) - H_2(t)\|.$$

The solution's positivity

State variables of model (1) and relative factors must be positive for the foreseeable future, as this model predicts the population of individuals, which will be established by the following theorem:

Theorem 2 *For model (1), the feasible area is specified by:*

$$\mathcal{C} = \left\{ (\mathfrak{S}_I, E_I, I, \mathcal{I}_{nd}, R, H) \in R_+^6; \middle| \ \mathfrak{S}_I, E_I, I, \mathcal{I}_{nd}, R, H \geq 0, N \leq \tfrac{\Pi}{\mu} \right\}.$$

Proof Count on the value of factors to be continuous. Predicting the following from system (1) is straightforward (see [26]):

$$\frac{d\mathfrak{S}_I}{dt} \geq -(\nu I + \theta + \mu)\mathfrak{S}_I.$$

After that, applying the constant variation formula:

$$\frac{d\mathfrak{S}_I}{dt} \geq \mathfrak{S}_I(0) \exp(-(\nu I + \theta + \mu)t) \geq 0.$$

In the same way, we prove that: $\frac{dE_I}{dt} \geq 0$, $\frac{dI}{dt} \geq 0$, $\frac{d\mathcal{I}_{nd}}{dt} \geq 0$, $\frac{dR}{dt} \geq 0$, $\frac{dH}{dt} \geq 0$. As a result, when $t \geq 0$, all solutions are positive.
Or,

$$N = \mathfrak{S}_I + E_I + I + \mathcal{I}_{nd} + R + H.$$

Then we have

$$\frac{dN}{dt} = \Pi - \mu N(t) - \mu_1(I + \mathcal{I}_{nd}).$$

When the illness is absent

$$\frac{dN}{dt} = \Pi - \mu N(t),$$

then

$$\int \frac{dN}{dt} = \int (\Pi - \mu N(t))dt.$$

So

$$N(t) = N(0) \exp(-\int_0^t \mu ds) + \int_0^t \Pi \exp(-\int_s^t \mu d\vartheta),$$

if

$$N(0) \leq \frac{\Pi}{\mu},$$

thus,

$$N(t) \leq \frac{\Pi}{\mu}\exp(-\int_0^t \mu ds) + \int_0^t \Pi\exp(-\mu(t-s)ds) \leq \frac{\Pi}{\mu}\exp(-\int_0^t \mu ds) + \frac{\Pi}{\mu},$$

when

$$t \to +\infty, \qquad N(t) \leq \frac{\Pi}{\mu}.$$

It indicates that the region $\mathcal{C}$ is a positively invariant set for system (1).

Local stability of DFE

Because $H(t)$ has not been presented in the first five equations, system (1) can be expressed below

$$\begin{cases} \frac{d\mathfrak{S}_I}{dt} = \Pi - \nu\mathfrak{S}_I I - (\mu+\theta)\mathfrak{S}_I, \\ \frac{dE_I}{dt} = \nu\mathfrak{S}_I I - \delta E_I - \mu E_I, \\ \frac{dI}{dt} = \alpha\delta E_I - \eta I - (\mu+\mu_1)I, \\ \frac{d\mathcal{I}_{nd}}{dt} = (1-\alpha)\delta E_I - \gamma\mathcal{I}_{nd} - (\mu+\mu_1)\mathcal{I}_{nd}, \\ \frac{dR}{dt} = \eta I + \gamma\mathcal{I}_{nd} - \mu R. \end{cases} \tag{2}$$

The model's disease-free equilibrium point is reached by setting all of the model (2)'s formulas to zero and disabling them:

$$\mathcal{E}_0 = (\mathfrak{S}_I^0, E_I^0, I^0, \mathcal{I}_{nd}^0, R_0),$$

where $E_I = I = \mathcal{I}_{nd} = R = 0$, and $\mathfrak{S}_I^0 = \frac{\Pi}{\theta+\mu}$.

The effective reproduction number $\mathcal{R}_0$

The threshold provided by the dimensionless basic reproduction number is vital in determining whether the disease survives or disappears in the individual. $\mathcal{R}_0$ can be defined more broadly as the number of new infections produced by a typical infective population at an infection spot zero-point equilibrium analysis of the stability of the equilibrium points depends on the model's effective reproduction number. Moreover, the projected number of indirect connections caused by the implementation of a newly discovered member among a sensitive group is estimated using $\mathcal{R}_0$. Using the notion of a next-generation matrix (see [27]), it is possible to calculate the basic reproduction number $\mathcal{R}_0$. Starting with the categories that were most recently infected, we recast

the model's equations:

$$\begin{cases} \dfrac{dE_I}{dt} = \nu \mathfrak{S}_I I - (\delta + \mu) E_I, \\ \dfrac{dI}{dt} = \alpha\delta E_I - (\eta + \mu) I, \\ \dfrac{d\mathcal{I}_{nd}}{dt} = (1-\alpha)\delta E_I - (\gamma + \mu)\mathcal{I}_{nd}, \\ \dfrac{dR}{dt} = \eta I + \gamma \mathcal{I}_{nd} - \mu R. \end{cases} \tag{3}$$

Deriving the fundamental reproduction number $\mathcal{R}_0$ involves utilizing the spectrum's diameter ρ in the generation matrix FV^{-1}. In this process, we consider the non-negative matrix F and the non-singular matrix V, representing the creation of new infections and the transition component in the system (2), respectively.

$$\mathbb{F} = \begin{pmatrix} \nu I \mathfrak{S}_I \\ 0 \\ 0 \\ 0 \end{pmatrix}, \quad \text{and} \quad \mathbb{V} = \begin{pmatrix} (\delta + \mu) E_I \\ -\alpha\delta E_I + (\eta + \mu + \mu_1) I \\ -(1-\alpha)\delta E_I + (\gamma + \mu + \mu_1)\mathcal{I}_{nd} \\ -\eta I - \gamma \mathcal{I}_{nd} + \mu R \end{pmatrix},$$

as $F = [\frac{\partial \mathbb{F}}{\partial X_j}]$, and $V = [\frac{\partial \mathbb{V}}{\partial X_j}]$, we have $(X_j = (E_I, I, \mathcal{I}_{nd}, R))$

$$F = \frac{\partial \mathbb{F}}{\partial X_j}(\mathcal{E}_0) = \begin{pmatrix} 0 & \nu \mathfrak{S}_I^0 & 0 & 0 \\ 0 & 0 & 0 & 0 \\ 0 & 0 & 0 & 0 \\ 0 & 0 & 0 & 0 \end{pmatrix},$$

and

$$V = \frac{\partial \mathbb{V}}{\partial X_j}(\mathcal{E}_0) = \begin{pmatrix} (\delta + \mu) & 0 & 0 & 0 \\ -\alpha\delta & (\eta + \mu + \mu_1) & 0 & 0 \\ -(1-\alpha)\delta & 0 & (\gamma + \mu + \mu_1) & 0 \\ 0 & -\eta & -\gamma & \mu \end{pmatrix}.$$

We have

$$|V| = \mu(\gamma + \eta)(\eta + \mu)(\delta + \mu).$$

Then

$$com(V) = \begin{pmatrix} \mathfrak{w}_{11} & \mathfrak{w}_{12} & \mathfrak{w}_{13} & \mathfrak{w}_{14} \\ \mathfrak{w}_{21} & \mathfrak{w}_{22} & \mathfrak{w}_{23} & \mathfrak{w}_{24} \\ \mathfrak{w}_{31} & \mathfrak{w}_{32} & \mathfrak{w}_{33} & \mathfrak{w}_{34} \\ \mathfrak{w}_{41} & \mathfrak{w}_{42} & \mathfrak{w}_{43} & \mathfrak{w}_{44} \end{pmatrix},$$

with

$$\begin{aligned}
\mathfrak{w}_{11} &= \mu(\eta+\mu+\mu_1)(\gamma+\mu+\mu_1),\\
\mathfrak{w}_{12} &= \mu(\gamma+\mu+\mu_1)\alpha\delta,\\
\mathfrak{w}_{13} &= \mu(1-\alpha)\delta(\eta+\mu+\mu_1),\\
\mathfrak{w}_{14} &= \eta(\gamma+\eta)\alpha\delta+\gamma(1-\alpha)\delta(\eta+\mu),\\
\mathfrak{w}_{22} &= \mu(\delta+\mu)(\gamma+\mu+\mu_1),\\
\mathfrak{w}_{23} &= -\mu,\\
\mathfrak{w}_{24} &= \eta(\gamma+\mu+\mu_1)(\delta+\mu),\\
\mathfrak{w}_{32} &= -\mu,\\
\mathfrak{w}_{33} &= \mu(\delta+\mu)(\eta+\mu+\mu_1),\\
\mathfrak{w}_{34} &= \gamma(\delta+\mu)(\eta+\mu+\mu_1),\\
\mathfrak{w}_{44} &= (\gamma+\mu+\mu_1)(\delta+\mu)(\eta+\mu+\mu_1),\\
\mathfrak{w}_{21} &= \mathfrak{w}_{31} = \mathfrak{w}_{41} = \mathfrak{w}_{42} = \mathfrak{w}_{43} = 0,
\end{aligned}$$

then

$$\begin{aligned}
V^{-1} &= \frac{1}{|V|}\begin{pmatrix}
\mathfrak{w}_{11} & \mathfrak{w}_{21} & \mathfrak{w}_{31} & \mathfrak{w}_{41}\\
\mathfrak{w}_{12} & \mathfrak{w}_{22} & \mathfrak{w}_{32} & \mathfrak{w}_{42}\\
\mathfrak{w}_{13} & \mathfrak{w}_{23} & \mathfrak{w}_{33} & \mathfrak{w}_{43}\\
\mathfrak{w}_{14} & \mathfrak{w}_{24} & \mathfrak{w}_{34} & \mathfrak{w}_{44}
\end{pmatrix}\\
&= \frac{1}{|V|}\begin{pmatrix}
\mu(\eta+\mu+\mu_1)(\gamma+\mu+\mu_1) & 0 & 0 & 0\\
\mu(\gamma+\mu+\mu_1)\alpha\delta & \mu(\delta+\mu)(\gamma+\mu+\mu_1) & -\mu & 0\\
\mu(1-\alpha)\delta(\eta+\mu+\mu_1) & -\mu & \mathfrak{w}_{33} & 0\\
\varsigma_1 & \varsigma_2 & \varsigma_3 & \varsigma_4
\end{pmatrix},
\end{aligned}$$

$$\begin{aligned}
\varsigma_1 &= \eta(\gamma+\mu)\alpha\delta+\gamma(1-\alpha)\delta(\eta+\mu+\mu_1),\\
\varsigma_2 &= \eta(\gamma+\mu+\mu_1)(\delta+\mu),\\
\varsigma_3 &= \gamma(\delta+\mu)(\eta+\mu+\mu_1),\\
\varsigma_4 &= (\gamma+\mu+\mu_1)(\delta+\mu)(\eta+\mu+\mu_1),
\end{aligned}$$

thus

$$FV^{-1} = \frac{1}{|V|}\begin{pmatrix}
\nu\mathfrak{S}_I^0\mathfrak{w}_{12} & \nu\mathfrak{S}_I^0\mathfrak{w}_{22} & \nu\mathfrak{S}_I^0\mathfrak{w}_{32} & \nu\mathfrak{S}_I^0\mathfrak{w}_{42}\\
0 & 0 & 0 & 0\\
0 & 0 & 0 & 0\\
0 & 0 & 0 & 0
\end{pmatrix}.$$

Therefore, the reproduction number ($\mathcal{R}_0$) is given below:

$$\mathcal{R}_0 = \rho(FV^{-1}) = \frac{\nu\mathfrak{S}_I^0\mathfrak{w}_{12}}{|V|} = \frac{\nu\Pi\alpha\delta}{(\theta+\mu)(\eta+\mu+\mu_1)(\delta+\mu)}.$$

Theorem 3 *If $\mathcal{R}_0 < 1$, the DFE point is locally asymptotically stable; if $\mathcal{R}_0 > 1$, it is unstable.*

Proof To prove this theorem, we start the Jacobian matrix for the given set of equations in the model (2):

$$J = \begin{pmatrix} -(\nu I + \theta + \mu) & 0 & -\nu \mathfrak{S}_I & 0 & 0 \\ \nu I & -(\delta + \mu) & \nu \mathfrak{S}_I & 0 & 0 \\ 0 & \alpha\delta & -(\eta + \mu + \mu_1) & 0 & 0 \\ 0 & (1-\alpha)\delta & 0 & -(\gamma + \mu + \mu_1) & 0 \\ 0 & 0 & \eta & \gamma & -\mu \end{pmatrix}. \tag{4}$$

Calculating the Jacobean matrix (4) at the point $\mathcal{E}_0$ yields the next results:

$$J(\mathcal{E}_0) = \begin{pmatrix} -(\theta + \mu) & 0 & -\frac{\nu\Pi}{\theta+\mu} & 0 & 0 \\ 0 & -(\delta + \mu) & \frac{\nu\Pi}{\theta+\mu} & 0 & 0 \\ 0 & \alpha\delta & -(\eta + \mu + \mu_1) & 0 & 0 \\ 0 & (1-\alpha)\delta & 0 & -(\gamma + \mu + \mu_1) & 0 \\ 0 & 0 & \eta & \gamma & -\mu \end{pmatrix}.$$

The next form of an eigenvalue polynomial has been computed by using the Jacobian matrix:

$$\mathfrak{P}(\lambda) = -(\mu + \lambda)(\theta + \mu)(\gamma + \mu + \mu_1 + \lambda)\bar{\mathfrak{P}}(\lambda), \tag{5}$$

where

$$\begin{aligned} \bar{\mathfrak{P}}(\lambda) &= (\delta + \mu + \lambda)(\eta + \mu + \mu_1 + \lambda) - \frac{\alpha\delta\nu\Pi}{\theta + \mu}, \\ &= \lambda^2 + \lambda(\eta + \mu + \mu_1 + \delta + \mu) + (\delta + \mu)(\eta + \mu + \mu_1) - \frac{\alpha\delta\nu\Pi}{\mu}. \end{aligned}$$

From equation (5), we have

$$\begin{aligned} \lambda_1 &= -\mu < 0, \\ \lambda_2 &= -(\gamma + \mu + \mu_1) < 0, \\ \lambda_3 &= -(\theta + \mu) < 0. \end{aligned}$$

From the expression of $\bar{\mathcal{P}}(\lambda)$, we have

$$\Delta = (\eta + \mu + \mu_1 + \delta + \mu)^2 + 4(\frac{\alpha\delta\nu\Pi}{\theta + \mu} - (\delta + \mu)(\eta + \mu + \mu_1) > 0.$$

As

$$\frac{\alpha\delta\nu\Pi}{\theta + \mu} \geq (\delta + \mu)(\eta + \mu + \mu_1), \text{ then } \Delta > 0.$$

Furthermore

$$\lambda_3 = -\frac{(\eta + \mu + \mu_1 + \delta + \mu) + \sqrt{\Delta}}{2} < 0, \quad \lambda_4 = \frac{-(\eta + \mu + \mu_1 + \delta + \mu) + \sqrt{\Delta}}{2},$$

$$\lambda_4 < 0 \text{ for } \Delta < (\eta + \mu + \mu_1 + \delta + \mu)^2,$$

means

$$\frac{\nu\Pi\alpha\delta}{\mathcal{R}_0(\theta+\mu)} > \frac{\alpha\delta\nu\Pi}{(\theta+\mu)} - \frac{(\delta+\mu+\eta+\mu+\mu_1)^2}{4},$$

then,

$$\frac{1}{\mathcal{R}_0} > 1 - \frac{(\delta+\mu+\eta+\mu+\mu_1)^2(\theta+\mu)}{4\nu\Pi\alpha\delta},$$

this implies, $\mathcal{R}_0 < 1$. Therefore, after using the Jacobian stability approach, $\mathcal{E}_0$ is locally asymptotically steadfast. If the initial population size of the affected individuals falls inside the lower set of the point $\mathcal{E}_0$, then the virus can be partially eradicated.

Global stability of DFEs

Theorem 4 *If $\mathcal{R}_0 < 1$, the DFE, $\mathcal{E}_0$ of model (2), is globally equilibrium-stable.*

Proof In this case, we shall use the system (1) since we need the vector X to be 2-dimensional at least. We have written equation system (1) based on [28, 29] in the following structure.

$$\begin{cases} \dfrac{dX}{dt} = \mathcal{M}(X - X_{\mathcal{E}_0,n}) + \mathcal{M}_1, \\ \dfrac{dY}{dt} = \mathcal{M}_2 Y, \end{cases} \tag{6}$$

where $Y = (E_I, I, \mathcal{I}_{nd}, R)$ is the proportion of people who are ill, $X_{\mathcal{E}_0,n}$ is a vector at the unaffected stability spot with the equal vector magnitude as X, and $X = (\mathfrak{S}_I, H)$ reflects the number of healthy people. By the above [28], For the free-of-illness equilibrium point $\mathcal{E}_0 = (\frac{\Pi}{\mu}, 0, 0, 0, 0, \frac{\Pi\theta}{\mu(\mu+\theta)})$ of system (1) to be globally asymptotically steady, several requirements must be satisfied:

1) The matrix $\mathcal{M}$ must have real negative eigenvalues.

2) $\mathcal{M}_2$ ought to be a Metzler matrix.

We have $X_{\mathcal{E}_0,n} = (\frac{\Pi}{\mu}, \frac{\Pi\theta}{\mu(\mu+\theta)})^T$.
The combination of Eq. (6) and Eq. (1) makes up the following system of equations:

$$\begin{pmatrix} \Pi - \nu\mathfrak{S}_I I - (\mu+\theta)\mathfrak{S}_I \\ \theta\mathfrak{S}_I - \mu H \end{pmatrix} = \mathcal{M} \begin{pmatrix} \mathfrak{S}_I - \frac{\Pi}{\theta+\mu} \\ H - \frac{\Pi\theta}{\mu(\theta+\mu)} \end{pmatrix} + \mathcal{M}_1 \begin{pmatrix} E_I \\ I \\ \mathcal{I}_{nd} \\ R \end{pmatrix},$$

and

$$\begin{pmatrix} \nu\mathfrak{S}_I I - (\delta+\mu)E_I \\ \alpha\delta E_I - (\eta+\mu+\mu_1)I \\ (1-\alpha)\delta E_I - (\gamma+\mu+\mu_1)\mathcal{I}_{nd} \\ \eta I + \gamma\mathcal{I}_{nd} - \mu R \end{pmatrix} = \mathcal{M}_2 \begin{pmatrix} E_I \\ I \\ \mathcal{I}_{nd} \\ R \end{pmatrix}.$$

The Jacobian matrix of the ensemble of Eq. (1) is the one below:

$$J(\mathcal{E}_0) = \begin{pmatrix} -(\mu+\theta) & 0 & -\frac{\nu\Pi}{\theta+\mu} & 0 & 0 & 0 \\ 0 & -(\delta+\mu) & \frac{\nu\Pi}{\theta+\mu} & 0 & 0 & 0 \\ 0 & \alpha\delta & -(\eta+\mu+\mu_1) & 0 & 0 & 0 \\ 0 & (1-\alpha)\delta & 0 & -(\gamma+\mu+\mu_1) & 0 & 0 \\ 0 & 0 & \eta & \gamma & -\mu & 0 \\ \theta & 0 & 0 & 0 & 0 & -\mu \end{pmatrix}.$$

The matrix $\mathcal{M}$, $\mathcal{M}_1$ and $\mathcal{M}_2$ are:

$$\mathcal{M} = \begin{pmatrix} -(\mu+\theta) & 0 \\ \theta & -\mu \end{pmatrix}, \quad \mathcal{M}_1 = \begin{pmatrix} 0 & -\frac{\nu\Pi}{\theta+\mu} & 0 & 0 \\ 0 & 0 & 0 & 0 \end{pmatrix},$$

and

$$\mathcal{M}_2 = \begin{pmatrix} -(\delta+\mu) & \frac{\nu\Pi}{\theta+\mu} & 0 & 0 \\ \alpha\delta & -(\eta+\mu+\mu_1) & 0 & 0 \\ (1-\alpha)\delta & 0 & -(\gamma+\mu+\mu_1) & 0 \\ 0 & \eta & \gamma & -\mu \end{pmatrix}.$$

Thus, all the roots of $\mathcal{M}$ have strictly negative real roots, and the matrix $\mathcal{M}_2$ is a Metzler matrix. Therefore the point, $\mathcal{E}_0$ is globally stable if $\mathcal{R}_0 < 1$.
Instead, we can use the Lyapunov function $\mathfrak{K}$ to prove the equilibrium global of the point, $\mathcal{E}_0$, where

$$\mathfrak{K} = \varkappa_1 E_I + \varkappa_2 I. \tag{7}$$

We chose this function meticulously because of its efficacy in examining the equilibrium of evolving structures with more intricate behavior. In which there are a pair of positive coefficients, $\varkappa_1$ and $\varkappa_2$.
If we differentiate Eq. (7) with respect to t, we find

$$\frac{d\mathfrak{K}}{dt} = \varkappa_1 \frac{dE_I}{dt} + \varkappa_2 \frac{dI}{dt}.$$

By replacing $\frac{dE_I}{dt}$, and $\frac{dI}{dt}$ of template (2), we have:

$$\frac{d\mathfrak{K}}{dt} = (\varkappa_1 \nu \mathfrak{S}_I - (\eta+\mu+\mu_1)\varkappa_2) I + (\alpha\delta\varkappa_2 - (\delta+\mu)\varkappa_1) E_I.$$

In this case, we take $\varkappa_1 = \frac{\delta\alpha}{(\delta+\mu)}\varkappa_2$, then since $\mathfrak{S}_I < \mathfrak{S}_I^0$, we have:

$$\begin{aligned} \frac{d\mathfrak{K}}{dt} &= (\frac{\alpha\delta\nu}{\delta+\mu}\mathfrak{S}_I - (\eta+\mu+\mu_1))\varkappa_2 I \\ &< (\frac{\alpha\delta\nu}{\delta+\mu}\mathfrak{S}_I^0 - (\eta+\mu+\mu_1))\varkappa_2 I. \end{aligned}$$

Taking $\varkappa_2 = 1$, and substituting $\mathcal{R}_0$, we get

$$\frac{d\mathfrak{K}}{dt} < (\mathcal{R}_0 - 1)I.$$

So then, if and only if $I = 0$, $I < I^0$, and $\frac{d\mathfrak{K}}{dt} \leq 0$, for $\mathcal{R}_0 < 1$, and $\frac{d\mathfrak{K}}{dt} = 0$. As a consequence, in field $\mathcal{C}$, $\mathcal{E}_0$ evolves globally asymptotically steady by the LaSalle principle of invariance.

The persistent steadiness $\tilde{\mathcal{E}}$

There is a unique persistent stable $\tilde{\mathcal{E}}$ form of model (2) $\tilde{\mathcal{E}} = (\tilde{\mathfrak{S}}_I, \tilde{E}_I, \tilde{I}, \tilde{I}_{nd}, \tilde{R})$, from where $\tilde{\mathcal{E}}$ is the solution to the persistent steadiness of the ongoing virus in the community. We can achieve this by zeroing each equation in (2):

$$\frac{d\mathfrak{S}_I}{dt} = \frac{dE_I}{dt} = \frac{dI}{dt} = \frac{d\mathcal{I}_{nd}}{dt} = \frac{dR}{dt} = 0.$$

Then, we obtain

$$\tilde{\mathfrak{S}}_I = \frac{\Pi}{\theta + \mu + \nu\tilde{I}}, \quad \tilde{E}_I = \frac{\nu\Pi\tilde{I}}{(\delta + \mu)(\nu\tilde{I} + \theta + \mu)},$$

$$\tilde{I} = \frac{\alpha\delta\Pi}{(\eta + \mu + \mu_1)(\delta + \mu)} - \frac{\theta + \mu}{\nu} = (\mathcal{R}_0 - 1)(\theta + \mu), \tag{8}$$

$$\tilde{I}_{nd} = \frac{(1-\alpha)\delta\nu\Pi\tilde{I}}{(\gamma + \mu + \mu_1)(\delta + \mu)(\nu\tilde{I} + \theta + \mu)}, \quad \tilde{R} = \frac{\gamma(1-\alpha)\delta\nu\Pi\tilde{I}}{\mu(\gamma + \mu)(\delta + \mu)(\nu\tilde{I} + \theta + \mu)} + \frac{\eta}{\mu}\tilde{I}_{nd}.$$

All the expressions are in terms of the $\tilde{I}$, due to the non-negative assumption for all model parameters. Consequently, we arrived at the following result:

Lemma 1 *When $\mathcal{R}_0 > 1$, system (2) has a unique persistent steadiness (positive) but not otherwise.*

Theorem 5 *A singular persistent steadiness for the model (2) whenever $\mathcal{R}_0 > 1$, as signified by $\tilde{\mathcal{E}} = (\tilde{\mathfrak{S}}_I, \tilde{E}_I, \tilde{I}, \tilde{I}_{nd}, \tilde{R})$, where the expressions of $\tilde{\mathfrak{S}}_I$, $\tilde{E}_I$, $\tilde{I}$, $\tilde{I}_{nd}$ and $\tilde{R}$ are given in (8).*

Local stability of $\tilde{\mathcal{E}}$

Theorem 6 *If $\mathcal{R}_0 > 1$, the endemic equilibrium point $\tilde{\mathcal{E}}$ is locally asymptotically stable.*

Proof To validate the above theorem, let us derive the Jacobian matrix for model (2):

$$J = \begin{pmatrix} -(\nu I + \theta + \mu) & 0 & -\nu\mathfrak{S}_I & 0 & 0 \\ \nu I & -(\delta + \mu) & \nu\mathfrak{S}_I & 0 & 0 \\ 0 & \alpha\delta & -(\eta + \mu) & 0 & 0 \\ 0 & (1-\alpha)\delta & 0 & -(\gamma + \mu + \mu_1) & 0 \\ 0 & 0 & \eta & \gamma & -\mu \end{pmatrix}. \tag{9}$$

The characteristic polynomial for Eq. (9) at the specified point $\tilde{\mathcal{E}}$ is:

$$\mathfrak{A}(\lambda) = (\mu + \lambda)(\gamma + \mu + \mu_1 + \lambda)\bar{\mathcal{Q}}(\lambda), \tag{10}$$

$$\begin{aligned}\bar{\mathcal{Q}}(\lambda) &= -\lambda^3 - \lambda^2(\nu\tilde{I} + \theta + \delta + \eta + 3\mu) \\ &\quad -\lambda[(\nu\tilde{I} + \theta + \mu)(\delta + \mu) + (\nu\tilde{I} + \theta + \delta + 2\mu)(\eta + \mu + \mu_1) - \alpha\delta\nu\tilde{\mathfrak{S}}_I] \\ &\quad +\alpha\delta\nu\tilde{\mathfrak{S}}_I(\nu\tilde{I} + \theta + \mu) - [(\nu\tilde{I} + \theta + \mu)(\delta + \mu)(\eta + \mu + \mu_1) + \nu^2\alpha\delta{\tilde{\mathfrak{S}}_I}^2] \\ &= a_3\lambda^3 + a_2\lambda^2 + a_1\lambda + a_0,\end{aligned}$$

where

$$\begin{aligned}a_1 &= -[(\nu\tilde{I} + \theta + \mu)(\delta + \mu) + (\nu\tilde{I} + \theta + \delta + 2\mu)(\eta + \mu + \mu_1) - \alpha\delta\nu\tilde{\mathfrak{S}}_I], \\ a_2 &= -(\nu\tilde{I} + \theta + \delta + \eta + 3\mu + \mu_1), \\ a_0 &= \alpha\delta\nu\tilde{\mathfrak{S}}_I(\nu\tilde{I} + \theta + \mu) - [(\nu\tilde{I} + \theta + \mu)(\delta + \mu)(\eta + \mu + \mu_1) + \nu^2\alpha\delta{\tilde{\mathfrak{S}}_I}^2].\end{aligned}$$

From Eq. (10), we have

$$\begin{aligned}\lambda_1 &= -\mu < 0, \\ \lambda_2 &= -(\gamma + \mu + \mu_1) < 0.\end{aligned}$$

From the expression of $\bar{\mathcal{Q}}$, we have

$$a_0 + \lambda a_1 + \lambda^2 a_2 + a_3\lambda^3 = 0.$$

$$\begin{array}{c|ccc} \lambda^3 & a_3 & a_1 & 0 \\ \lambda^2 & a_2 & a_0 & 0 \\ \lambda & b_1 & 0 & 0 \end{array}$$

$$b_1 = -\frac{1}{a_2}\begin{vmatrix} a_3 & a_1 \\ a_2 & a_0 \end{vmatrix} = \frac{a_1a_2 + a_0}{a_2} = -\frac{\alpha\delta\nu(\nu\tilde{I}+\theta+\mu) - [\nu\tilde{I}+\theta+\mu)(\delta+\mu)(\eta+\mu+\mu_1) + \nu^2\alpha\delta{\tilde{\mathfrak{S}}_I}^2]}{(\nu\tilde{I}+\theta+\delta+\eta+3\mu+\mu_1)} - \zeta,$$

where

$$\zeta = [\nu\tilde{I} + \theta + \mu)(\delta + \mu) + (\nu\tilde{I} + \theta + \delta + 2\mu)(\eta + \mu + \mu_1) - \alpha\delta\tilde{\mathfrak{S}}_I].$$

Applying the Routh-Hurwitz criteria, it is determined that the real root of Eq. (5) is strictly non-negative iff $a_2 < 0$ and $b_1 < 0$. Clearly, we see that $a_2 < 0$ because it is the sum of positive parameters and we have $b_1 < 0$ if $\mathcal{R}_0 > \nu\Pi(\frac{\nu\tilde{I}}{\theta+\mu} + 1) > 1$.
Hence, the persistent steadiness $\tilde{\mathcal{E}}$ is locally indicating asymptotic steadiness.

Global stability of the point $\tilde{\mathcal{E}}$

Theorem 7 *The only endemic steady state of* (2) *exhibits global asymptotic steady when* $\mathcal{R}_0 > 1$.

Proof Consider the following Lyapunov function, which is commonly used and discussed in [30]:

$$\eth(\wp) = \wp - 1 - ln(\wp).$$

$\eth(\wp)$ is non-negative in $\in R_+^5$ except at $\wp = 1$, where it become zero. Then,

$$\mathfrak{T}(\mathfrak{S}_I, I) = \varkappa_1 \tilde{\mathfrak{S}}_I \eth(\frac{\mathfrak{S}_I}{\tilde{\mathfrak{S}}_I}) + \varkappa_2 \tilde{I} \eth(\frac{I}{\tilde{I}}). \tag{11}$$

Let $\varkappa_1 > 0$ and $\varkappa_2 > 0$ be positive constants to be determined subsequently. Clearly, $\mathfrak{T}$ is C^1, $\mathfrak{T}(\tilde{\mathcal{E}}) = 0$, and $\mathfrak{T}$ is positively nonzero at other locations.
Differentiating the equation with respect to t, we get

$$\frac{d\mathfrak{T}(\mathfrak{S}_I, I)}{dt} = \varkappa_1 (1 - \frac{\tilde{\mathfrak{S}}_I}{\mathfrak{S}_I}) \frac{d\mathfrak{S}_I}{dt} + \varkappa_2 (1 - \frac{\tilde{I}}{I}) \frac{dI}{dt}. \tag{12}$$

By substituting $\frac{d\mathfrak{S}_I}{dt}$ and $\frac{dI}{dt}$ in model (2), we obtain,

$$\begin{aligned} \frac{d\mathfrak{T}}{dt} =& \frac{\varkappa_1}{\mathfrak{S}_I}(\mathfrak{S}_I - \tilde{\mathfrak{S}}_I)(\Pi - (\nu I + \mu)\mathfrak{S}_I) + \frac{\varkappa_2}{I}(I - \tilde{I})(\alpha\delta E_I - (\eta + \mu + \mu_1)I) \\ <& \varkappa_1 \frac{(\mathfrak{S}_I - \tilde{\mathfrak{S}}_I)}{\mathfrak{S}_I}\Pi - \varkappa_1(\nu I + \mu)(\mathfrak{S}_I - \tilde{\mathfrak{S}}_I) + \frac{\varkappa_2(I - \tilde{I})\alpha\delta E_I)}{I}. \end{aligned}$$

For $\varkappa_1 = \frac{\mathfrak{S}_I(I-\tilde{I})}{(\mathfrak{S}_I - \tilde{\mathfrak{S}}_I)}$ and $\varkappa_2 = 1$, we find,

$$\begin{aligned} \frac{d\mathfrak{T}}{dt} &< (\Pi - \frac{\mathcal{R}_0(\eta + \mu + \mu_1)(\delta + \mu)(\theta + \mu)\mathfrak{S}_I}{\alpha\delta\Pi} - (\theta + \mu)\mathfrak{S}_I + \frac{\alpha\delta E_I}{I})(I - \tilde{I}) \\ &< (\Pi - \frac{\mathcal{R}_0(\eta + \mu + \mu_1)(\delta + \mu)(\theta + \mu)\mathfrak{S}_I}{\alpha\delta\Pi} + \frac{\alpha\delta E_I}{I})(I - \tilde{I}). \end{aligned}$$

Thus, $\frac{d\mathfrak{T}}{dt} < 0$ only if, $\mathcal{R}_0 > \frac{\Pi^2\alpha\delta}{(\eta+\mu+\mu_1)(\delta+\mu)(\theta+\mu)}$, and $\frac{d\mathfrak{T}}{dt} \leq 0$ if $I = \tilde{I}$, then the point, $\tilde{\mathcal{E}}$ is globally asymptotically stable.

5 Exploring the responsiveness of the model variables to $\mathcal{R}_0$

The examination of structure sensitivity is applied to calculate the difference in implementation speed due to changes in strategy variables. Implementation effort is assumed to be a differentiable function of structure, at most undersized in the proximity of the current strategy point. Moreover, To suggest the most appropriate methods to decrease human permanence and illness, it is essential to understand the relative importance of the numerous factors that influence the new coronavirus's spread. Further, it permits us to determine how a condition variable varies correspondingly whenever a system factor adapts. Since the first spread of illness is restricted to the rate $\mathcal{R}_0$, we calculate the sensitivity indicators about these factors of system (2). Thus, we construct the next sensitivity factor [31, 32]:

$$\mathfrak{F}_x^{\mathcal{R}_0} = \frac{\partial\mathcal{R}_0}{\partial x}\frac{x}{\mathcal{R}_0}.$$

Table 2. Sensitivity indicators

Setting symbol	Index of sensitivity
μ	-0.8463
δ	+0.1176
Π	+1
ν	+1
η	-0.8366
α	+1
μ	-0.6423
θ	-0.8789

$$
\begin{aligned}
\mathfrak{F}_{\mu}^{\mathcal{R}_0} &= -\frac{(3\mu^2+2\mu(\theta+\eta+\delta+\mu_1)+\theta\eta+(\theta+\eta)\delta)\mu}{(\theta+\mu)(\eta+\mu+\mu_1)(\delta+\mu)},\\
\mathfrak{F}_{\eta}^{\mathcal{R}_0} &= -\frac{\eta}{\eta+\mu+\mu_1},\\
\mathfrak{F}_{\delta}^{\mathcal{R}_0} &= \frac{\mu}{(\delta+\mu)},\\
\mathfrak{F}_{\theta}^{\mathcal{R}_0} &= -\frac{\theta}{\theta+\mu},\\
\mathfrak{F}_{\mu_1}^{\mathcal{R}_0} &= -\frac{\mu_1}{\eta+\mu+\mu_1},\\
\mathfrak{F}_{\nu}^{\mathcal{R}_0} &= 1,\\
\mathfrak{F}_{\Pi}^{\mathcal{R}_0} &= 1,\\
\mathfrak{F}_{\alpha}^{\mathcal{R}_0} &= 1.
\end{aligned}
$$

We have, $\mathfrak{F}_{\delta}^{\mathcal{R}_0}, \mathfrak{F}_{\Pi}^{\mathcal{R}_0}, \mathfrak{F}_{\nu}^{\mathcal{R}_0}, \mathfrak{F}_{\alpha}^{\mathcal{R}_0} > 0$ while, $\mathfrak{F}_{\mu}^{\mathcal{R}_0}, \mathfrak{F}_{\eta}^{\mathcal{R}_0}, \mathfrak{F}_{\mu_1}^{\mathcal{R}_0}, \mathfrak{F}_{\theta}^{\mathcal{R}_0} < 0$. It implies that $\mathcal{R}_0$ is reduced in μ and η but raised in δ, Π, ν and α, while $\mathfrak{F}_{\gamma}^{\mathcal{R}_0} = 0$ since $\mathcal{R}_0$ does not rely on γ.

6 Expansion to an optimal control problem

In this section, we provide an effective control technique that will aid governments in developing nations in regaining control of the circumstances at the lowest possible price. Researchers are constantly seeking effective ways to prevent the spread of new viruses, including vaccination, isolation, and quarantine. However, isolation and quarantine procedures can reduce and eradicate the impact of the virus in the absence of effective vaccination. Thus, from [33] the controlled model results in:

$$
\begin{cases}
\dfrac{d\mathfrak{S}_I}{dt} = \Pi - \nu(1-\mathfrak{v}_1)\mathfrak{S}_I I - (\mu+\theta)\mathfrak{S}_I,\\
\dfrac{dE_I}{dt} = \nu(1-\mathfrak{v}_1)\mathfrak{S}_I I - \delta(1-\mathfrak{v}_2)E_I - \mu E_I,\\
\dfrac{dI}{dt} = \alpha\delta(1-\mathfrak{v}_2)E_I - (\eta+\mu+\mu_1)I - \mathfrak{v}_2 I,\\
\dfrac{d\mathcal{I}_{nd}}{dt} = (1-\alpha)\delta(1-\mathfrak{v}_2)E_I - (\gamma+\mu+\mu_1)\mathcal{I}_{nd} - \mathfrak{v}_2\mathcal{I}_{nd},\\
\dfrac{dR}{dt} = \eta I + \gamma\mathcal{I}_{nd} + \mathfrak{v}_2(I+\mathcal{I}_{nd}) - \mu R.
\end{cases}
\tag{13}
$$

To sample the methods of control and affect its influence in Morocco, we raise in the model a two controls variable that represents a comprehensive approach to prevention, including personal hygiene, social isolation, and creating sensitivity across all midpoints, to keep the virus away from people vulnerable to infection, and treatment support for infectious diseases (as the best care for sick people in isolation institutions), denoted by $\mathfrak{v}_1$ and $\mathfrak{v}_2$, respectively. The value $\mathfrak{v}_1(t) = 0$ denotes that no isolation measure is performed, while the value 1 corresponds to full effort on preventing the infectious disease. The value $\mathfrak{v}_2(t) = 0$ signifies the absence of treatment support, and $\mathfrak{v}_2(t) = 1$ represents the effective application of the treatment to reduce the propagation of COVID-19.
In the model, we pursue the $\mathfrak{v}_1$ and $\mathfrak{v}_2$ values that downplay the functionally objective subject to the differential Eq. (14). The supplied objective functional is:

$$J(\mathfrak{v}_1, \mathfrak{v}_2) = \int_0^T (I(t) + \mathcal{I}_{nd}(t) + \frac{\varpi_1}{2}\mathfrak{v}_1^2(t) + \frac{\varpi_2}{2}\mathfrak{v}_2^2(t))dt. \tag{14}$$

Consider

$$\Lambda = (\mathfrak{S}_I, E_I, I, \mathcal{I}_{nd}, R), \quad \mathfrak{v} = (\mathfrak{v}_1, \mathfrak{v}_2), \quad \mathfrak{v} = (\mathfrak{v}_1, \mathfrak{v}_2),$$

and

$$\wp(t, \Lambda, \mathfrak{v}) = I(t) + \mathcal{I}_{nd}(t) + \frac{\varpi_1}{2}\mathfrak{v}_1^2(t) + \frac{\varpi_2}{2}\mathfrak{v}_2^2(t),$$

if the relative cost factors $\varpi_1 > 0$ and $\varpi_2 > 0$ are available. They are selected to contrast the respective strengths of $\mathfrak{v}_1(t)$ and $\mathfrak{v}_2(t)$ at instant t, where T is the final instance. Or, we want to find the optimal controls $\mathfrak{v}_1^*$ and $\mathfrak{v}_2^*$, where,

$$J(\mathfrak{v}_1^*, \mathfrak{v}_2^*) = \min_{\mathfrak{v}_1, \mathfrak{v}_2 \; in U} J(\mathfrak{v}_1, \mathfrak{v}_2). \tag{15}$$

With, $\digamma$ defined as the subset of eligible controls

$$\digamma = \left\{ \mathfrak{v}_1, \mathfrak{v}_2 \in \digamma \middle| \; 0 \leq \mathfrak{v}_1(t) \leq 1 \; and \; 0 \leq \mathfrak{v}_1(t) \leq 1, t \in [0, T] \right\}. \tag{16}$$

Existence of the optimal controls

Here, we demonstrate the existence of such ideal control functions that lower prices in a limited time. For this purpose, we stick to the results presented in [34].

Theorem 8 *In set $\digamma$, there is an optimal control couple, $\mathfrak{v}_1^*$ and $\mathfrak{v}_2^*$ with $J(\mathfrak{v}_1^*, \mathfrak{v}_2^*) = \min_{\mathfrak{v}_1, \mathfrak{v}_2 \in \digamma} J(\mathfrak{v}_1, \mathfrak{v}_2)$ relating to the control system (13-14).*

Proof The following conditions should be fulfilled as stated in (Theorem 4.1 pg. 68 in [35]):

a) In the case of the system (13) with control variables in $\digamma$, the set of solutions is non-void.
b) The steadier approach can be defined as a linear function of the control coefficients with factors set on the term and value of the parameters since the set $\digamma$ is closed and convex.
c) The integral of the function $\wp$ is convex in the domain $\digamma$, and the function $\wp(t, \Lambda, \mathfrak{v}) \geq \wp(\mathfrak{v})$,

where $\wp$ is a continuous function that realizes the following property:

$$|\mathfrak{v}|^{-1}\wp(\mathfrak{v}) \underset{\mathfrak{v}\to\infty}{\longrightarrow} \infty,$$

where $|.|$ indicates the classical Euclid norm.

Since $\lim_{t\to\infty} N(t) \leq \frac{\Pi}{\mu}$, then, all solutions of system (13) are bounded in $\digamma$. For each of the bounded control variables in $\digamma$, the system (13)'s solutions are bound. The system's (13) right-hand side functions meet the Lipschitz criterion about state variables. As a result, condition (a) is satisfied according to the Picard-Lindelöf theorem (see [36]). $\digamma$ satisfies the requirement of being closed and convex by definition. With coefficients that rely on state variables, the system (13) is linear in the control variable $\mathfrak{v}$. So, we accomplish condition (b).
According to the biquadratic and quadratic nature of the control variable $\mathfrak{v}$, $\int_0^T \wp(t,\Lambda,\mathfrak{v})dt$ is convex and $\wp(t,\Lambda,\mathfrak{v}) = I(t) + \mathcal{I}_{nd}(t) + \frac{\varpi_1}{2}\mathfrak{v}_1^2(t) + \frac{\varpi_2}{2}\mathfrak{v}_2^2(t) \geq \frac{\varpi_1}{2}\mathfrak{v}_1^2(t) + \frac{\varpi_2}{2}\mathfrak{v}_2^2(t)$. After selecting $\wp(u) = \mathfrak{w}_1(\mathfrak{v}_1^2 + \mathfrak{v}_2^2)$, where $\mathfrak{w}_1 = \min(\varpi_1, \varpi_2) > 0$, we get then $\wp(t, X, \mathfrak{v}) \geq \wp(\mathfrak{v})$. It is evident that $\wp(\mathfrak{v})$ is a continuous function and satisfies the condition $|\mathfrak{v}|^{-1}\wp(\mathfrak{v}) \to \infty$ when $\mathfrak{v} \to \infty$, which gives us condition (c). As a result, utilizing the findings from [34], the existence of the optimal control is confirmed.

Characterization of the optimal control

We use Pontryagin's maximum principle and the Hamiltonian at the time t defined to derive the requirements for optimal control:

$$\tilde{H} = I(t) + \mathcal{I}_{nd}(t) + \frac{\varpi_1}{2}\mathfrak{v}_1^2(t) + \frac{\varpi_2}{2}\mathfrak{v}_2^2(t) + \sum_{i=1}^{5} \lambda_i(t) f_i(\Lambda).$$

$\Lambda = (\mathfrak{S}_I, E_I, I, \mathcal{I}_{nd}, R)$ and the function f_i is the start of the (13) differences equations for the *ith* variable value.

Theorem 9 *In light of the state system solutions that reduce the impact of J on $\digamma$ and the optimal controls $\mathfrak{v}_1^*$, $\mathfrak{v}_2^*$ and $\mathfrak{S}_I, E_I, I, \mathcal{I}_{nd}$ and R, respectively, adjacent variables, such as $\lambda_1, \ldots, \lambda_5$, are used.*

$$\begin{aligned}
\frac{d\lambda_1}{dt} &= \lambda_1\nu(1-\mathfrak{v}_1)I + \lambda_1(\mu+\theta) - \lambda_2\nu(1-\mathfrak{v}_1)I,\\
\frac{d\lambda_2}{dt} &= \lambda_2\delta(1-\mathfrak{v}_2) + \lambda_2\mu - \lambda_3\alpha\delta(1-\mathfrak{v}_2) - \lambda_4(1-\alpha)\delta(1-\mathfrak{v}_2),\\
\frac{d\lambda_3}{dt} &= -1 + \lambda_1\nu(1-\mathfrak{v}_1)\mathfrak{S}_I - \lambda_2\nu(1-\mathfrak{v}_1)\mathfrak{S}_I + \lambda_3(\eta+\mu+\mu_1+\mathfrak{v}_2) - \lambda_5(\eta+\mathfrak{v}_2),\\
\frac{d\lambda_4}{dt} &= -1 + \lambda_4(\gamma+\mu+\mu_1) + \lambda_4\mathfrak{v}_2 - \lambda_5(\gamma+\mathfrak{v}_2),\\
\frac{d\lambda_5}{dt} &= \lambda_5\mu,
\end{aligned} \tag{17}$$

such as the requirements of transversality: $\lambda_{i=1,2,5}(t_f) = 0$ and $\lambda_{i=3,4}(t_f) = -1$.

Proof As well as

$$\tilde{H} = I(t) + \mathcal{I}_{nd}(t) + \frac{\varpi_1}{2}\mathfrak{v}_1^2(t) + \frac{\varpi_2}{2}\mathfrak{v}_2^2(t) + \sum_{i=1}^{5}\lambda_i(t)f_i(\Lambda),$$

where $f_1 = \Pi - \nu(1-\mathfrak{v}_1)\mathfrak{S}_I I - (\mu+\theta)\mathfrak{S}_I$, $f_2 = \nu(1-\mathfrak{v}_1)\mathfrak{S}_I I - \delta(1-\mathfrak{v}_2)E_I - \mu E_I$, $f_3 = \alpha\delta(1-\mathfrak{v}_2)E_I - (\eta+\mu+\mu_1)I - \mathfrak{v}_2 I$, $f_4 = (1-\alpha)\delta(1-\mathfrak{v}_2)E_I - (\gamma+\mu+\mu_1)\mathcal{I}_{nd} - \mathfrak{v}_2\mathcal{I}_{nd}$ and $f_5 = \eta I + \gamma\mathcal{I}_{nd} + \mathfrak{v}_2(I+\mathcal{I}_{nd}) - \mu R$.
The maximum principle of Pontryagin [37] is then applied, and we obtain,

$$\begin{aligned}
\frac{d\lambda_1}{dt} &= -\frac{\partial\tilde{H}}{\partial\mathfrak{S}_I} = \lambda_1\nu(1-\mathfrak{v}_1)I + \lambda_1(\mu+\theta) - \lambda_2\nu(1-\mathfrak{v}_1)I,\\
\frac{d\lambda_2}{dt} &= -\frac{\partial\tilde{H}}{\partial E_I} = \lambda_2\delta(1-\mathfrak{v}_2) + \lambda_2\mu - \lambda_3\alpha\delta(1-\mathfrak{v}_2) - \lambda_4(1-\alpha)\delta(1-\mathfrak{v}_2),\\
\frac{d\lambda_3}{dt} &= -\frac{\partial\tilde{H}}{\partial I} = -1 + \lambda_1\nu(1-\mathfrak{v}_1)\mathfrak{S}_I - \lambda_2\nu(1-\mathfrak{v}_1)\mathfrak{S}_I + \lambda_3(\eta+\mu+\mu_1+\mathfrak{v}_2) - \lambda_5(\eta+\mathfrak{v}_2),\\
\frac{d\lambda_4}{dt} &= -\frac{\partial\tilde{H}}{\partial\mathcal{I}_{nd}} = -1 + \lambda_4(\gamma+\mu+\mu_1) + \lambda_4\mathfrak{v}_2 - \lambda_5(\gamma+\mathfrak{v}_2),\\
\frac{d\lambda_5}{dt} &= -\frac{\partial\tilde{H}}{\partial R} = \lambda_5\mu.
\end{aligned} \tag{18}$$

The accompanying optimal controls $\mathfrak{v}_1^*$ and $\mathfrak{v}_2^*$ are thus established from $\frac{\partial\tilde{H}}{\partial\mathfrak{v}_1} = 0$, and $\frac{\partial\tilde{H}}{\partial\mathfrak{v}_2} = 0$. In light of this, we developed the characteristic equation involving the control boundary limits in the type of proposed control argument as follows:

$$\begin{aligned}
\mathfrak{v}_1^* &= \min\left\{1, \max(0, \frac{\nu\mathfrak{S}_I^* I^*(\lambda_2-\lambda_1)}{\varpi_1})\right\},\\
\mathfrak{v}_2^* &= \min\left\{1, \max(0, \frac{\lambda_3\alpha\delta E_I^* + \lambda_3 I^* + \lambda_4(1-\alpha)\delta E_I^* - \lambda_2\delta E_I^*}{\varpi_2})\right\}.
\end{aligned} \tag{19}$$

7 Discussions and numerical simulation

Without numerical validation of the statistics, the analytical study cannot be considered complete. To trace the behavior of the framework (2), we have shown some numerical simulations in this part for a variety of initial circumstances and parameters found in Table 3 and Table 4. Thus, we employed the fourth order RK technique in Matlab program to solve this issue. We considered the variables stated in Table 3 as well as the various beginning condition values provided in Table 4. Applying the fourth-order Runge-Kutta technique and the system's present solution round, the adjoint Eq. (17) is solved backward in time. These factors were used to estimate the reproduction number, and the results show that $\mathcal{R}_0 = 0.2132654$. Figure 2 makes it abundantly evident that the system's solution profiles converge to the disease-free state, with $\mathcal{E}_0 = (0.059\times10^7, 0, 0, 0, 0)$. The endemic equilibrium is asymptotically stable as determined by Theorem 7 when the value of α is changed to 0.0002, as seen in Figure 3. Or, the system's solution of (2) converges to $\tilde{\mathcal{E}} = (1.1234\times10^7, 0.7000\times10^7, 1.3476\times10^7, 1.5632\times10^7, 2.1000\times10^7, 3.1000\times10^7)$. Figure 4 demonstrates how the class H maintains stability and advances to the virus-free equilibrium point when $\mathcal{R}_0 < 1$ for each of the three various starting values of H. Figure 5 clearly shows that our solution for the classes I and E_I converges to $\mathcal{E}_0$ for $\mathcal{R}_0 < 1$ and is asymptotically stable. Figure 6 illustrates how the two classes I and E_I for the three distinct initial circumstances become stable at

the point, $\tilde{\mathcal{E}}$, when $\mathcal{R}_0 > 1$. Figure 7 shows how the population $\mathcal{I}_{nd}$ is asymptotically stable and converges to $\mathcal{E}_0$ when $\mathcal{R}_0 < 1$ (case 1), while the same class remains stable and converges to $\tilde{\mathcal{E}}$ in case $\mathcal{R}_0 > 1$ (case 2). Figure 8 shows the same category, but this time for the class R. We can see that system (2)'s solution is stable and converges to $\mathcal{E}_0$ in all three starting values of the recovered class when $\mathcal{R}_0 < 1$, but with the same beginning values of R and $\alpha = 0.210$, so that $\mathcal{R}_0 > 1$ the solution converges to $\tilde{\mathcal{E}}$. The theoretical findings of the local and global asymptotic stability of the endemic and disease-free equilibrium described in the preceding parts are, in sum, supported by all of the results of this section.

Furthermore, we use a fourth-order Runge-Kutta technique for the numeric estimation of the extremum provided by Theorem 8. With a forward fourth-order Runge-Kutta scheme and the transversality requirements $\lambda_{i=1,2,5}(t_f) = 0$ and $\lambda_{i=3,4}(t_f) = -1$, while, $\mathfrak{S}_I = \frac{\mathfrak{S}_I}{N}$, $E_I = \frac{E_I}{N}$, $I = \frac{I}{N}$, $\mathcal{I}_{nd} = \frac{\mathcal{I}_{nd}}{N}$ and $R = \frac{R}{N}$. This iterative approach solves the system in Eq. (13) with an estimate for the controls across the period interval $[0, T]$. A convex pair of the preceding controls and the results from (19), together with the current controls, for upgrading the controls. If the coefficients of the unresolved from the prior iteration are substantially similar to the ones from the present execution, the iteration is over. Concerning the digital simulations, we use $\mathfrak{v}_{\max} = 0.5$, with the end time value of $T = 1$ (months) plus the predetermined variables from Table 3, and with the following starting conditions:

$$\mathfrak{S}_I(0) = 0.4, \quad E_I(0) = 0.2, \quad I(0) = 0.17, \quad \mathcal{I}_{nd}(0) = 0.11 \quad \text{and} \quad R(0) = 0.5. \tag{20}$$

In Figure 9, when we use the technique $\mathfrak{v}_2$, we notice a reduction in the infected population. Only the control $\mathfrak{v}_1$, is employed (Strategy$_1$). The goal of this plan is to safeguard more people from COVID-19. Figure 10 shows a reduction in the number of people exposed, causing a decline in the count of individuals affected, which underlines the need to raise public awareness of the seriousness of the COVID-19 virus through preventive measures such as frequent manual hygiene, especially after snatching, and the use of safety covers to restrict the spread of the virus. The results in Figure 11 indicate that Strategy$_2$ reduces the number of people with the virus. The main objective of this procedure is to prevent the disease from spreading, which confirms that the essential purpose of therapy is to prevent the spread of the coronavirus. Furthermore, we observe a substantial reduction in the quantity of those infected with the two types of I and Ind when we incorporate the optimal control $\mathfrak{v}_1$ and $\mathfrak{v}_2$ (Strategy$_3$). Such is because stringent precautions, like isolation with therapy, occur, as depicted in Figure 12, and the approach also depends on sensitization efforts. It is clear that the controls implemented in this numerical simulation function well by reducing the population of diseased people and augmenting the number of cured people. Thus, we notice that the number of retrieved persons rises when we employ two distinct approaches. Additionally, we discovered, as shown in Figure 13, that there is an appealing correlation between $\mathcal{R}_0$ and the illness transmission coefficient in all afflicted groups, and this correlation is called α. This implies that α is the most important factor that needs to be decreased in order to regulate infections and lessen coronavirus. Our model relies on available epidemiological data, which may be subject to reporting bias or variations in screening capacity from one region to another. Moreover, the dynamic nature of the COVID-19 pandemic introduces uncertainties that may impact the accuracy of our forecasts. We have made assumptions about the homogeneity of the population and the uniformity of intervention measures, which may not fully reflect the complexity of real scenarios. In addition, the model considers simplified transmission dynamics without taking into account potential variations in viral strains or the influence of emerging variants. While we aim to provide valuable information, we recognize that

these simplifications and assumptions are necessary trade-offs and may influence the accuracy of our results. Future iterations of this model should incorporate more nuanced data and refine assumptions to improve accuracy and applicability.

Table 3. The baseline factor's value for the system (2)

factor	Value	Source
ν	0.9031	Presumption
α	0.4110	[25]
Π	20.000	Presumption
δ	$1/7day^{-1}$	[38]
η	0.1130	Presumption
μ	$0.0062day^{-1}$	[25]
θ	0.021	Presumption
ϖ_1	30	Assumption
ϖ_2	80	Assumption

Table 4. The beginning values for the system'(2)s factors

Starting values	State 1	State 2	State 3
N	397405	401405	360530
$\mathfrak{S}_I(0)$	163638	173638	118763
$E_I(0)$	93507	94507	95507
$I(0)$	70130	71130	72130
$\mathcal{I}_{nd}(0)$	46753	47753	48753
$R(0)$	23377	24377	25377

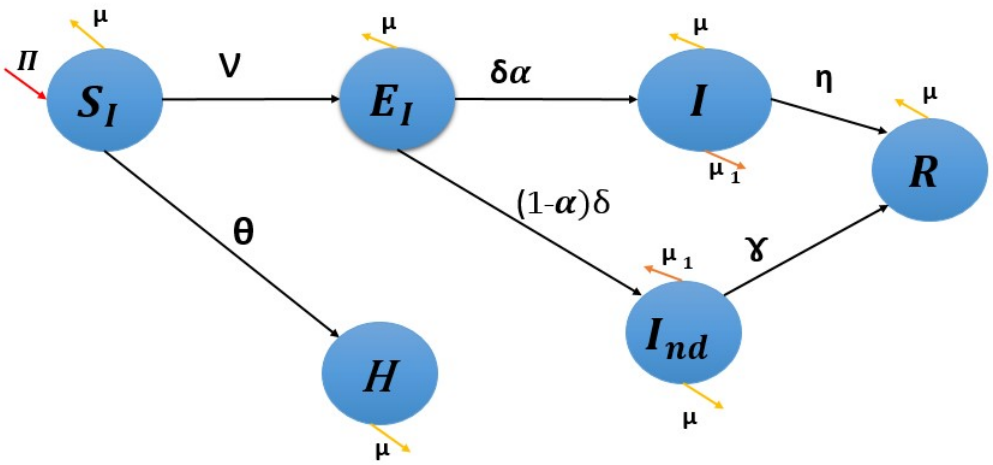

Figure 1. Prototype (1)'s diagram, or $\nu = \frac{\beta \mathfrak{S}_I I}{1+\sigma I}$

8 Cost-effectiveness

A mathematical technique called cost-effectiveness is used to establish if an intervention's benefits outweigh its costs. So, cost-effectiveness is a methodology to evaluate which intervention provides the highest value for the associated price. The value of an intervention in a cost-effectiveness analysis is measured using quantity-adjusted life years, also known as Qualis. Simply put, this is a generic measure of the burden of disease that includes not only quantity but also quality of life

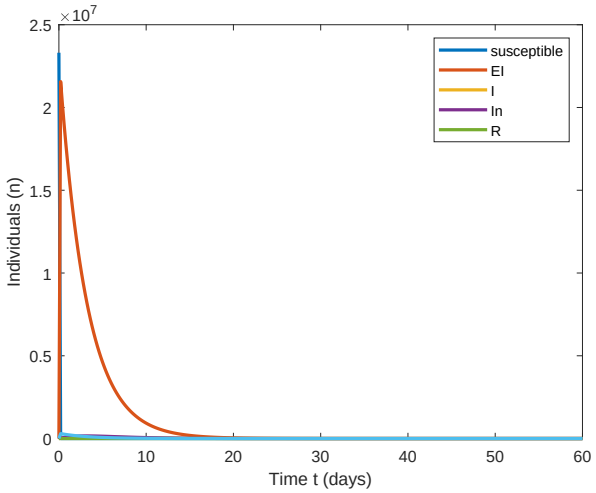

(a) Case 1

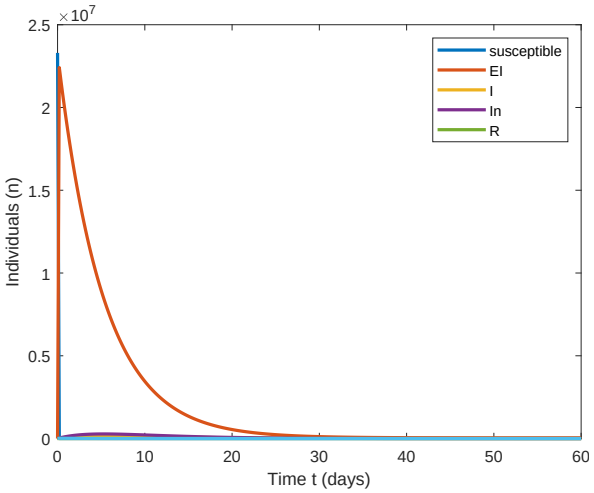

(b) Case 2

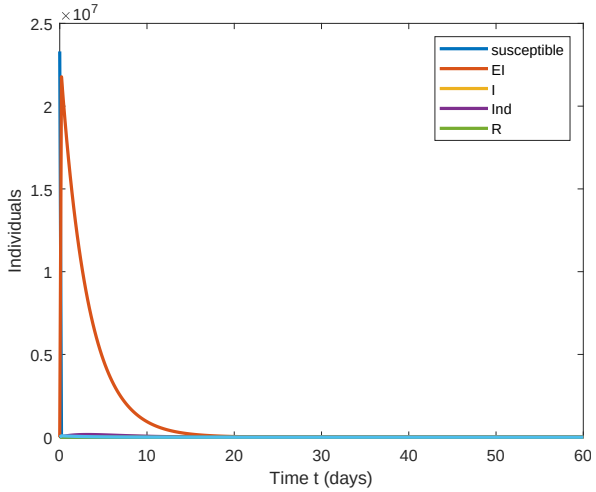

(c) Case 3

Figure 2. This figure shows that the unaffected steady-state framework (2) is $(2.180 \times 10^7, 0, 0, 0, 0)$.

after the intervention. This technique compares the cost and the effect of two interventions, and it is summarized using an incremental cost-effectiveness ratio, also known as an ISA. The total expense incurred during the whole duration is:

$$\varsigma(\mathfrak{v}) = \int_0^T (\varsigma(\mathfrak{v}_1, \mathfrak{v}_2))dt = \int_0^T \frac{\varpi_1}{2}\mathfrak{v}_1^2(t) + \frac{\varpi_2}{2}\mathfrak{v}_2^2(t))dt. \tag{21}$$

The incremental cost-effectiveness ratio (ICER) is expressed as follows (see [39]):

$$ICER = \frac{\text{Difference in costs of interventions } \mathfrak{v}_1 \text{ and } \mathfrak{v}_2}{\text{Difference in effect of interventions } \mathfrak{v}_1 \text{ and } \mathfrak{v}_2}.$$

This ratio shows the incremental costs over incremental quality-adjusted life years between the two comparators.

To be more precise, considering two concurrent strategies, $\mathcal{B}_1$ and $\mathcal{B}_2$, where Strategy $\mathcal{B}_2$ is more efficient than Strategy $\mathcal{B}_1$ ($TA(\mathcal{B}_1) < TA(\mathcal{B}_2)$), Implement ideas in [40–43]. ICER rates are

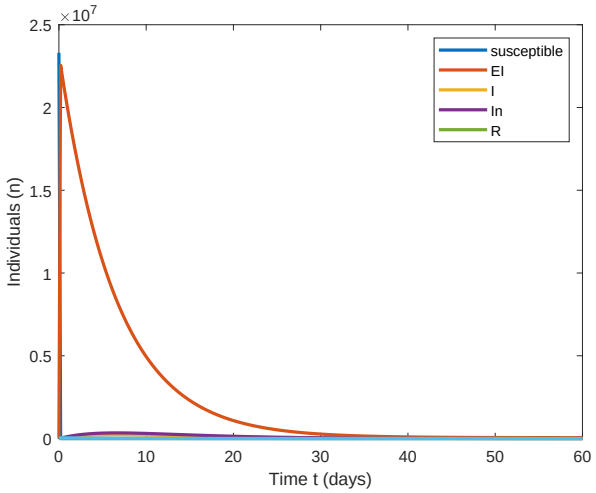

(a) Case 1

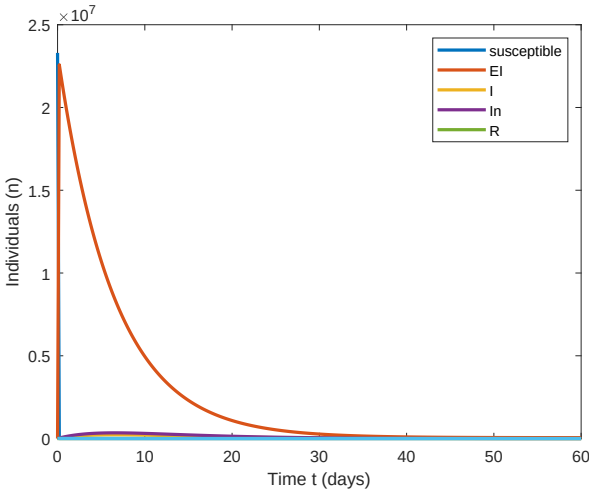

(b) Case 2

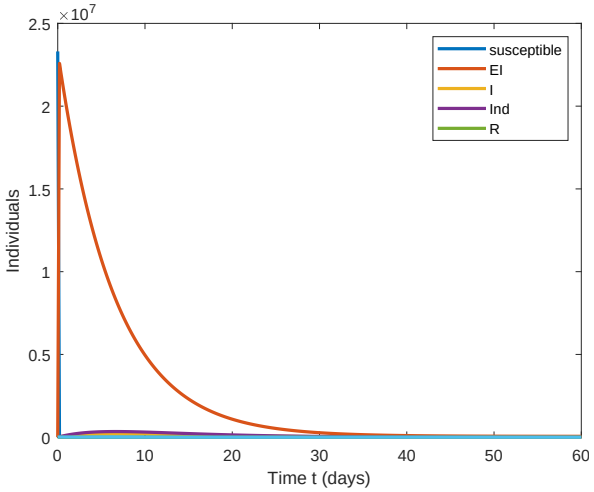

(c) Case 3

Figure 3. This figure shows that the persistent steadiness of model (2) is $(2.5468 \times 10^7, 0.9096 \times 10^7, 3.65859 \times 10^7, 1.7484 \times 10^7, 1.0857 \times 10^7, 3.6583 \times 10^7)$.

computed via the following equations:

$$ICER(\mathcal{B}_1) = \frac{TC(\mathcal{B}_1)}{TA(\mathcal{B}_1)}, \tag{22}$$

$$ICER(\mathcal{B}_2) = \frac{TC(\mathcal{B}_2) - TC(\mathcal{B}_1)}{TA(\mathcal{B}_2) - TA(\mathcal{B}_1)}. \tag{23}$$

In our analysis, the total expenditures (TC) and the total incidents prevented (TA) for the approach selected i for $i = 1, 2$, and 3 are defined as follows during a specific duration:

$$TC(\mathcal{B}_1) = \sum_{t=0}^{T-1} \varpi_1 \mathfrak{v}_1^*(E_I + \mathfrak{S}) + \varpi_2 \mathfrak{v}_1^*(I + \mathcal{I}_{nd}), \tag{24}$$

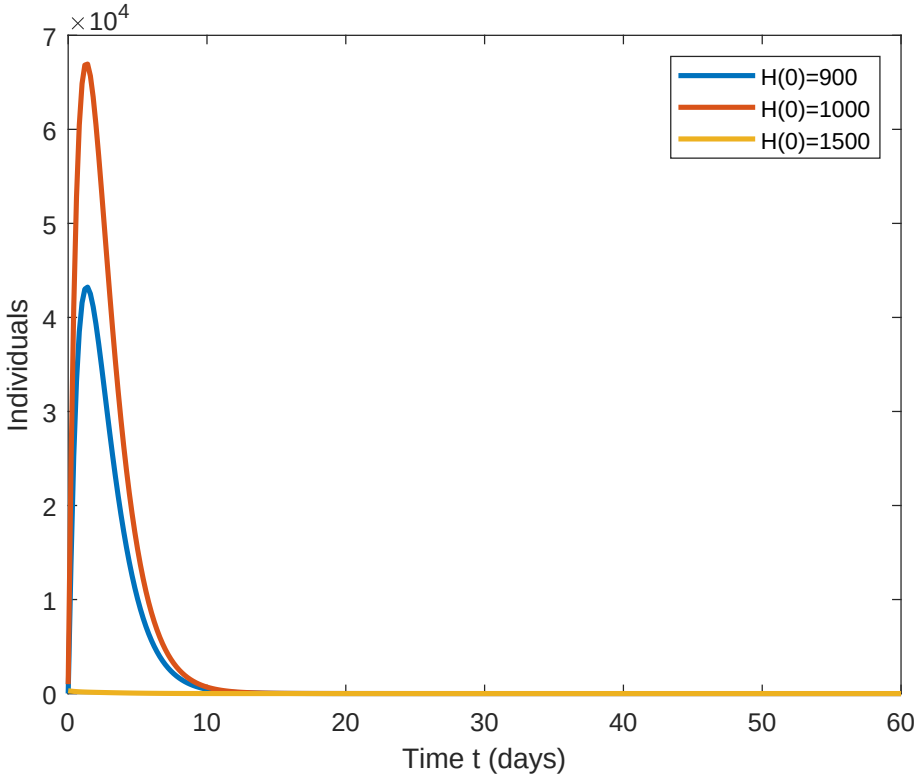

Figure 4. The model's digital solutions for the variables and various starting points of H, where $\mathcal{R}_0 = 0.0143613$. The equilibrium of the point $\mathcal{E}_0$ is stable.

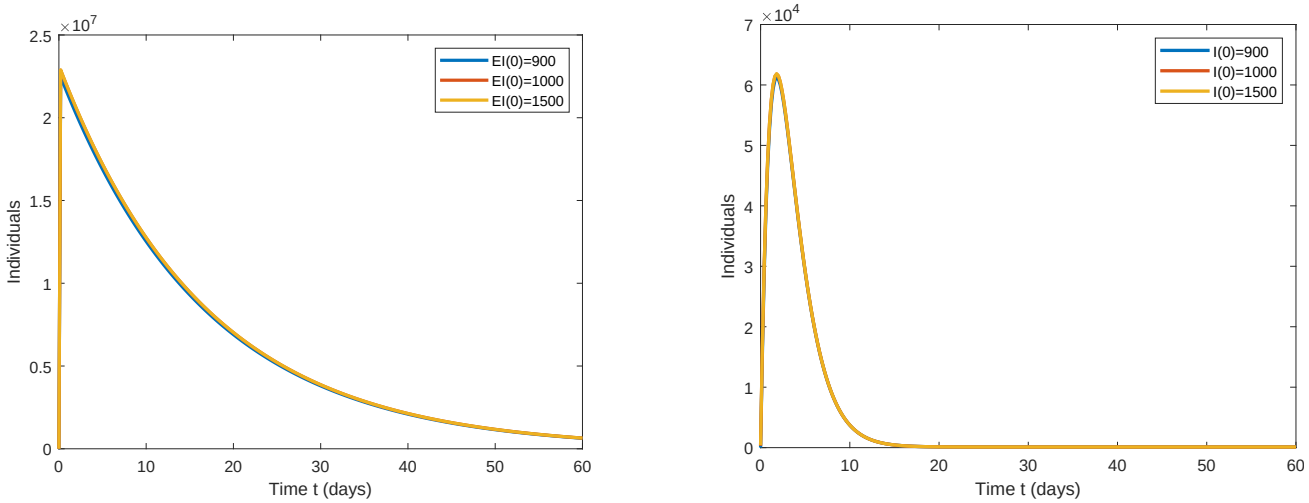

(a) Case 1 **(b)** Case 2

Figure 5. The model (2) numerical solutions for the factors and various starting conditions of E_I and I listed in Table 3 and Table 4, with the rate $\mathcal{R}_0 = 0.1352631$.

$$TA(\mathcal{B}_1) = \sum_{t=0}^{T} I + \mathcal{I}_{nd} - (I^* + \mathcal{I}^*_{nd}). \tag{25}$$

where I^* and $\mathcal{I}^*_{nd}$ represent the optimal solution linked to the optimal controls $\mathfrak{v}^*_1$ and $\mathfrak{v}^*_2$, while ϖ_1 and ϖ_2 represent the person-unit costs of the two potential interventions. We ordered our control measures in Table 2 according to the higher number of cases avoided under the template's computations.

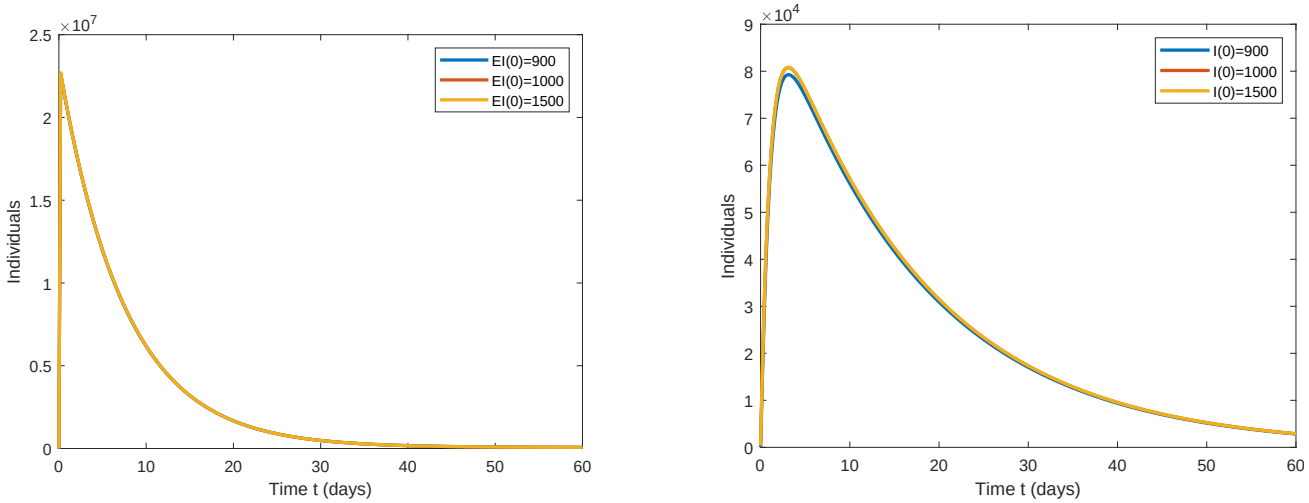

(a) Case 1 **(b)** Case 2

Figure 6. The system (2) numerical solutions for the parameters and various starting conditions of E_I and I listed in Table 3 and Table 4, here $\mathcal{R}_0 = 2.272166591341701$, the point $\tilde{\mathcal{E}}$ remains steady as well.

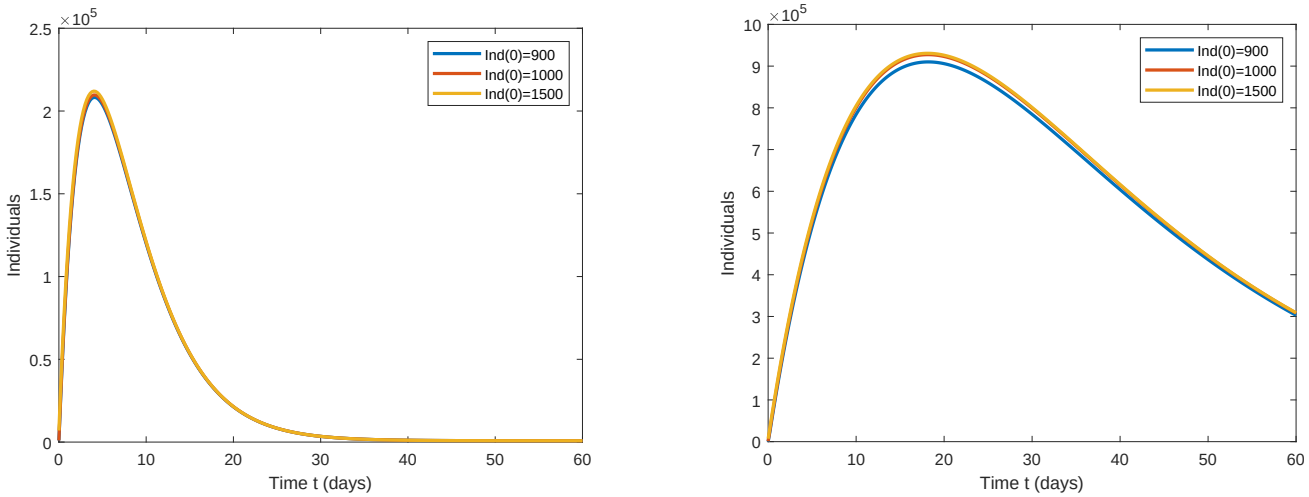

(a) Case 1 **(b)** Case 2

Figure 7. Digital solutions of the system (2) for factors and diverse starting state of $\mathcal{I}_{nd}$, here $\mathcal{R}_0 = 0.1352631$ in Case 1 and $\mathcal{R}_0 = 2.272166591341701$ in Case 2.

Strategy$_1$ (Processing $\mathfrak{v}_1$): Encourage the population to adopt a comprehensive approach to prevention, which includes self-care, social separation, and the sensitization of all levels, to keep the virus away from people vulnerable to infection.
Strategy$_2$ (Processing $\mathfrak{v}_2$): Control of infectious disorders therapy support (as the finest care for ill patients in isolation facilities).
Strategy$_3$ (Processing $\mathfrak{v}_1$ and $\mathfrak{v}_2$): Integrating Strategy$_1$ and Strategy$_2$ and employing controls $\mathfrak{v}_1$ and $\mathfrak{v}_2$. Based on the simulation results, we have ranked our control techniques in Table 3 according to the number of diseases avoided and given in Eq. (20). Table 2 compares Strategy $\mathcal{B}_1$ and Strategy $\mathcal{B}_2$ in terms of increased efficiency. In terms of improved efficiency, Strategy$_1$ and

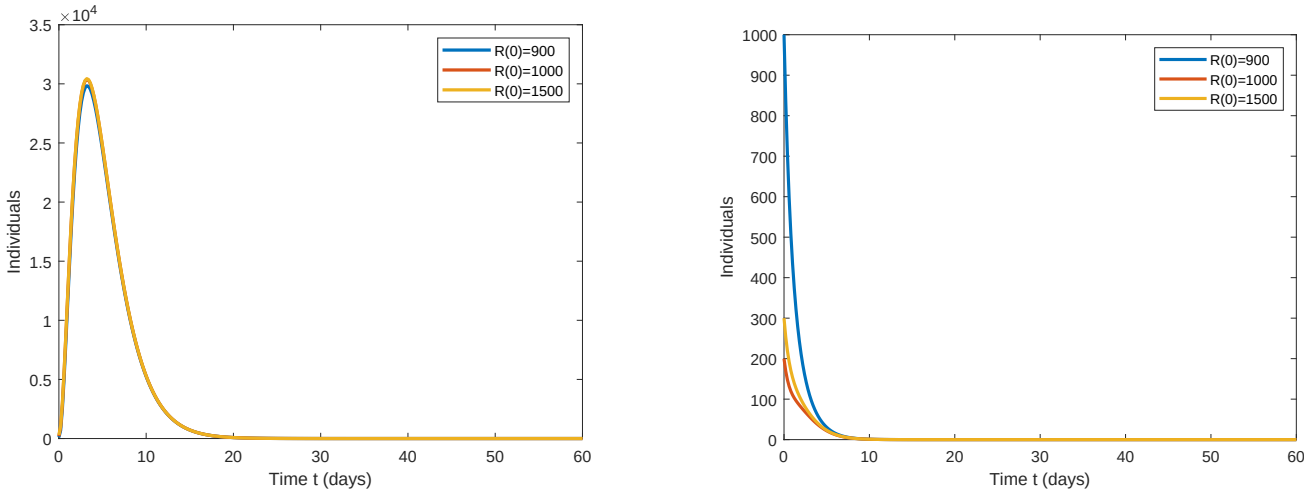

(a) Case 1 **(b)** Case 2

Figure 8. For parameters and various beginning conditions of R, numerical solutions of the model (2) are presented in Table 3 and Table 4, where $\mathcal{R}_0 = 3.193363191340714$ in Case 2, and $\mathcal{R}_0 = 0.2132654$ in Case 1

.

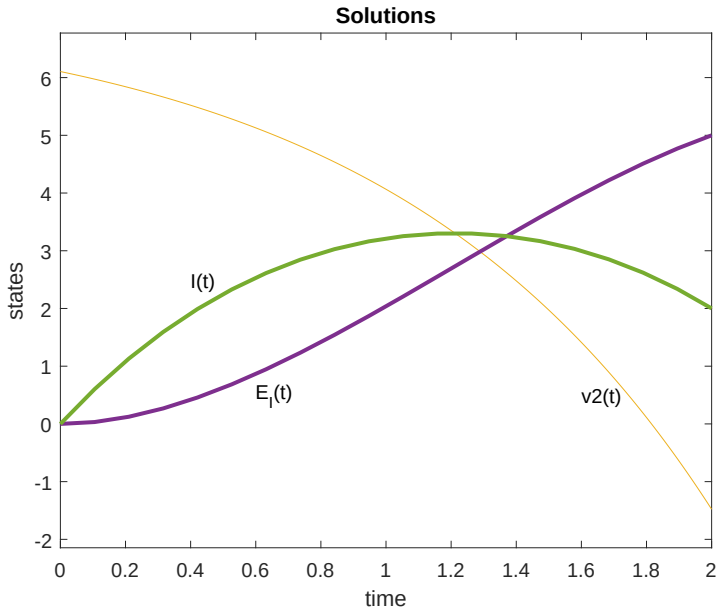

Figure 9. Application of the Strategy $\mathfrak{v}_2$

Strategy$_2$ are contrasted. The ICER values are calculated as follows:

$$\begin{aligned} ICER(1) &= \frac{TC(1)}{TA(1)} = \frac{1.73 \times 10^2}{3 \times 10^2} = 0.57, \\ ICER(2) &= \frac{TC(2) - TC(1)}{TA(2) - TA(1)} = \frac{1.9 \times 10^2 - 1.73 \times 10^2}{3.03 \times 10^2 - 3 \times 10^2} = 39. \end{aligned} \tag{26}$$

$ICER(2)$ is superior to $ICER(1)$. This indicates that plan (1) is more dominant than plan (2). Consequently, Strategy$_2$ is not featured in the list of options.

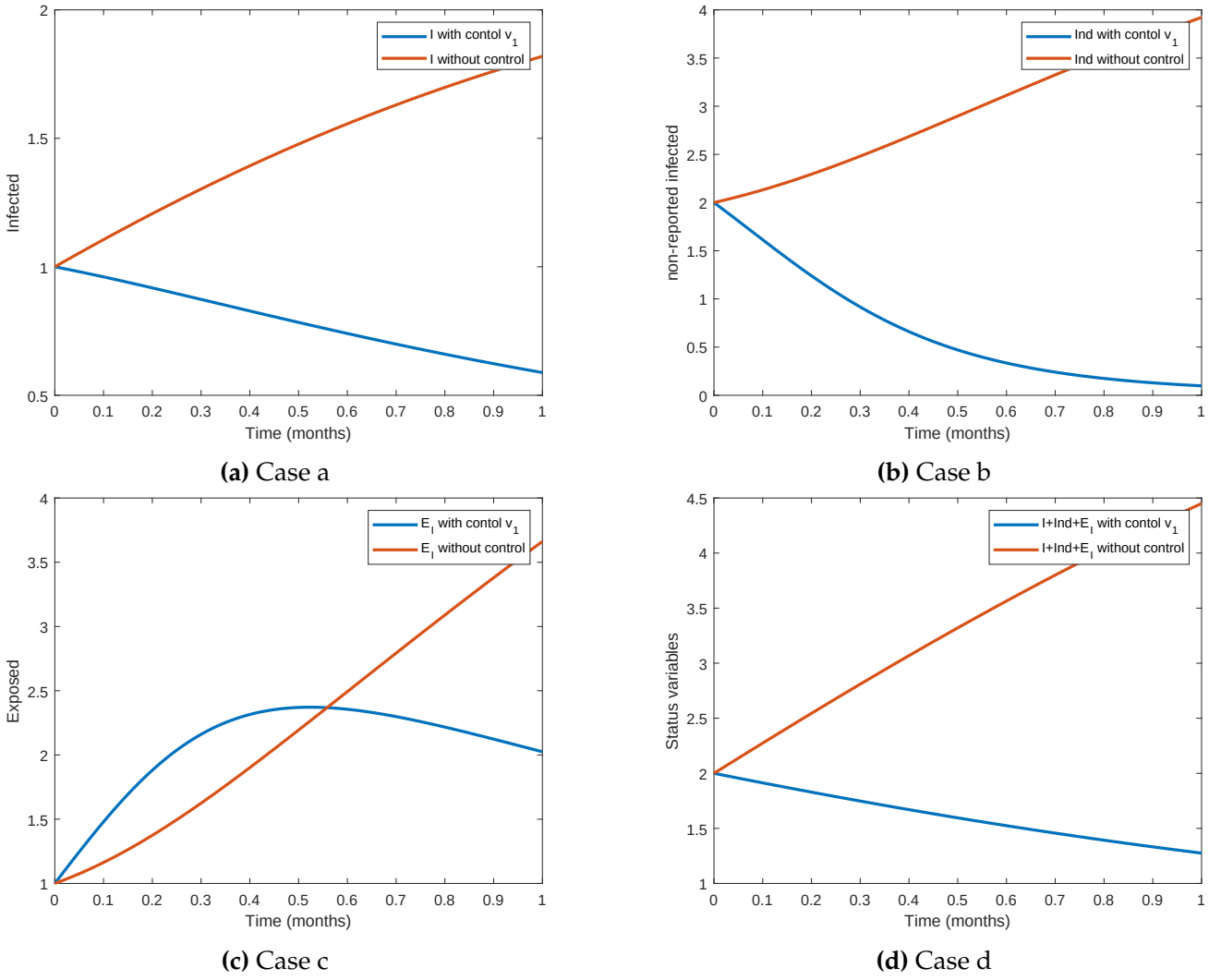

(a) Case a **(b)** Case b

(c) Case c **(d)** Case d

Figure 10. The progression of the number of individuals with control $\mathfrak{v}_1$

Next, we examined how cost-effective Strategy$_1$ and Strategy$_3$ were:

$$\begin{aligned} ICER(3) &= \frac{TC(3)}{TA(3)} = \frac{1.52 \times 10^2}{2.5 \times 10^2} = 0.608, \\ ICER(1) &= \frac{TC(1) - TC(3)}{TA(1) - TA(3)} = \frac{1.73 \times 10^2 - 1.52 \times 10^2}{3 \times 10^2 - 2.5 \times 10^2} = 0.42. \end{aligned} \tag{27}$$

According to the analysis, Strategy$_1$ is more affordable than Strategy$_3$. Consequently, method 1 is the most advantageous of all the strategies evaluated, as it is simultaneously approachable and healthy.

Table 5. Total expenses and total illnesses prevented across all techniques

Strategy	**TA**	**TC**
1	3×10^2	1.73×10^2
2	3.03×10^2	1.9×10^2
3	2.5×10^2	1.52×10^2

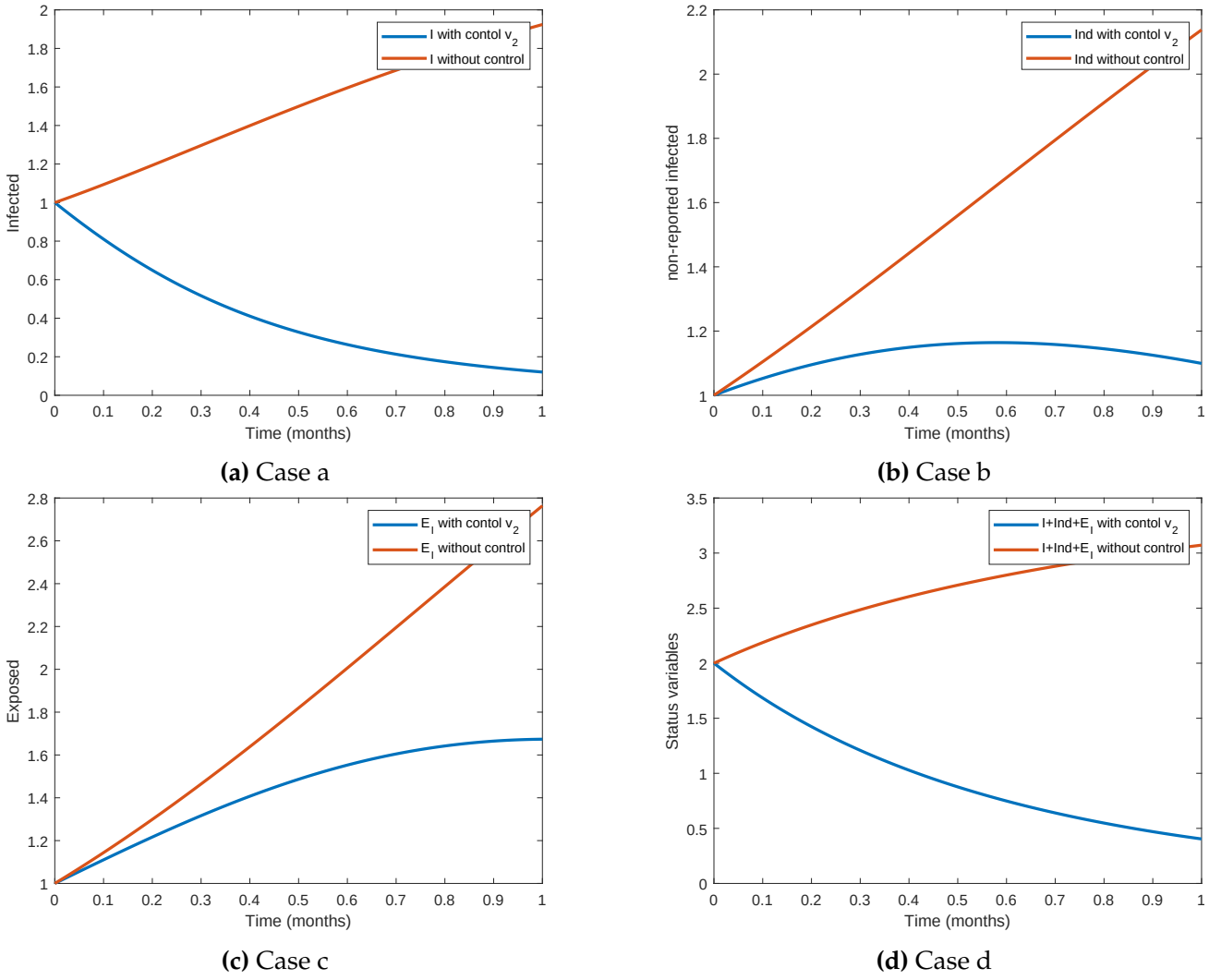

(a) Case a **(b)** Case b

(c) Case c **(d)** Case d

Figure 11. The progression of the number of individuals with control $\mathfrak{v}_2$

9 Conclusion

Multiple models have been proposed for the analysis of the COVID-19 pandemic. In this sample, we have highlighted the distinctive properties of COVID-19 and suggested an approach that explains how the virus transformed in Morocco while providing a reasonable representation of the actual pandemic in that country. The model's objective is to investigate the process of COVID-19 transmission while accounting for both reported and undeclared infections. These two categories were necessary, as many people have not reported their infection with the COVID-19 virus or even failed to take the necessary precautions to limit the spread of the virus and protect others, we also included a class of individuals who never got infected by COVID-19 (compartment H).
We suggest a compartmental epidemic model for newly emerging coronavirus infections, which considers COVID-19 infection to be a contagious disease. The dynamics of the interaction among the groups can be expressed mathematically by a framework of ODEs. We prove the solution's existence and uniqueness and compute the rate $\mathcal{R}_0$, which assisted in illustrating the equilibrium's stability. One can distinguish between what is globally stable and what is asymptotically stable. Similarly, the study uses the idea of normalized forward sensitivity to highlight the significance of every factor for the spread of COVID-19. We investigate the optimal control problem numerically in further detail, and our results show that the control strategies implemented reduce the prevalence of the virus in society during the period of the interaction. Moreover, we examined

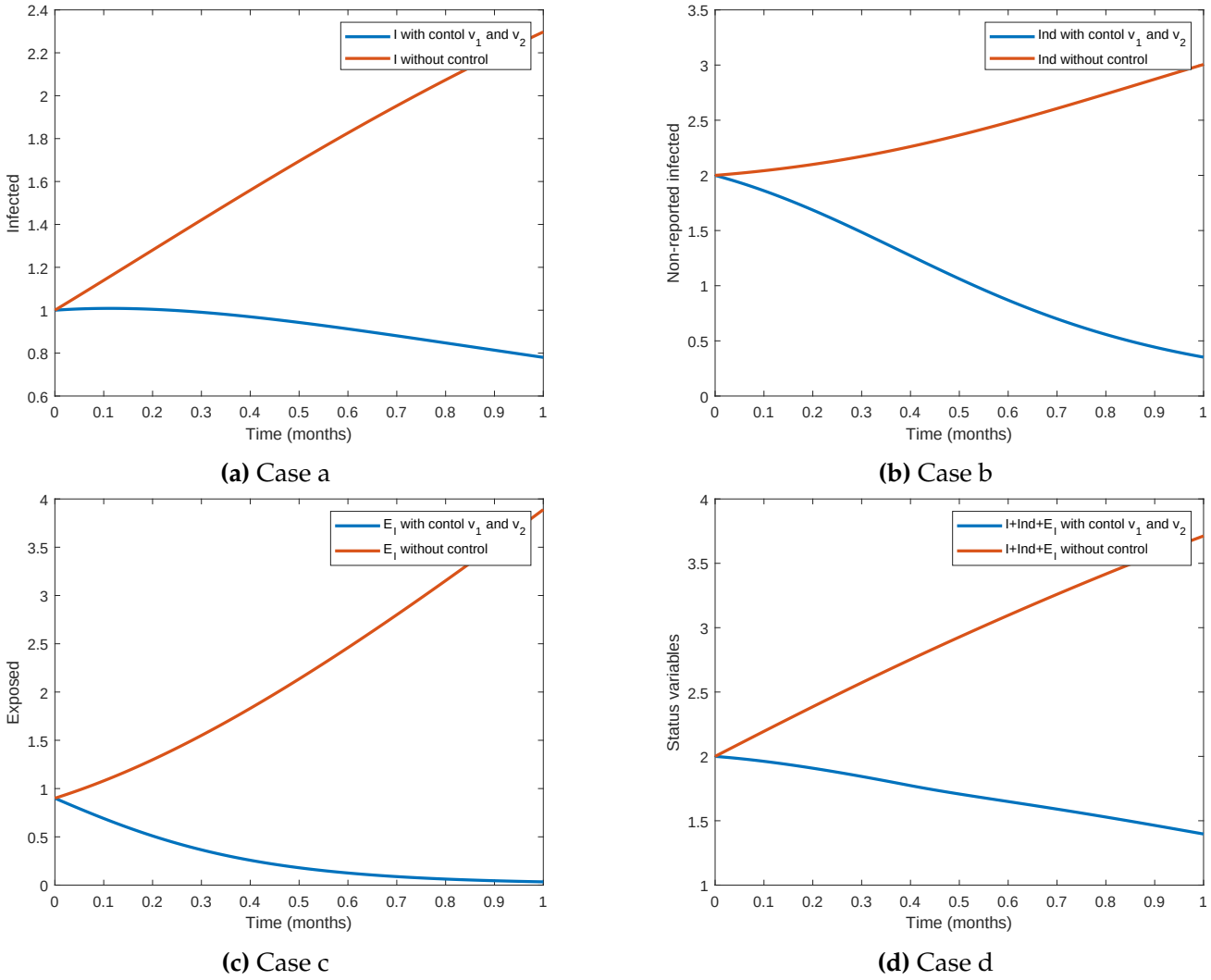

(a) Case a **(b)** Case b

(c) Case c **(d)** Case d

Figure 12. The admissible control set in Eq. (16), the starting factors in Eq. (20), and the optimal state values for the control problem in Eqs. (13)—(15), in contrast to control-free trajectories

the cost-effectiveness of control measures to determine the best way to manage COVID-19 while consuming as few resources as possible. We demonstrate, via the ICER cost-effectiveness approach, that while approach 3 (which promotes applying the two control $\mathfrak{v}_1$ and $\mathfrak{v}_2$) is the most effective, it does not minimize disease. In terms of cost, approach 2 (apply the control $\mathfrak{v}_2$) is the most expensive. Nevertheless, this tactic shows remarkable results in controlling disease transmission and reducing infection rates. Despite the high cost of this method, the Moroccan government is committed to adopting it. Likewise, it is essential to keep spreading the word about the value of immunization and prevention while stepping up efforts to target those who follow the guidelines and motivate them to share their understanding of and adherence to them. Ultimately, the 4th-order Runge-Kutta forward-backwards method in Matlab is used for numerical simulations to validate the analytical results. As a further work, we plan to use fractional calculus in our subsequent work and add more aspects to our analysis in future research, as it can provide a more precise description of natural occurrences than can be achieved using conventional differential. It can entail cooperation with experts in epidemiology, sociology, economics, and other relevant fields to create more comprehensive models.

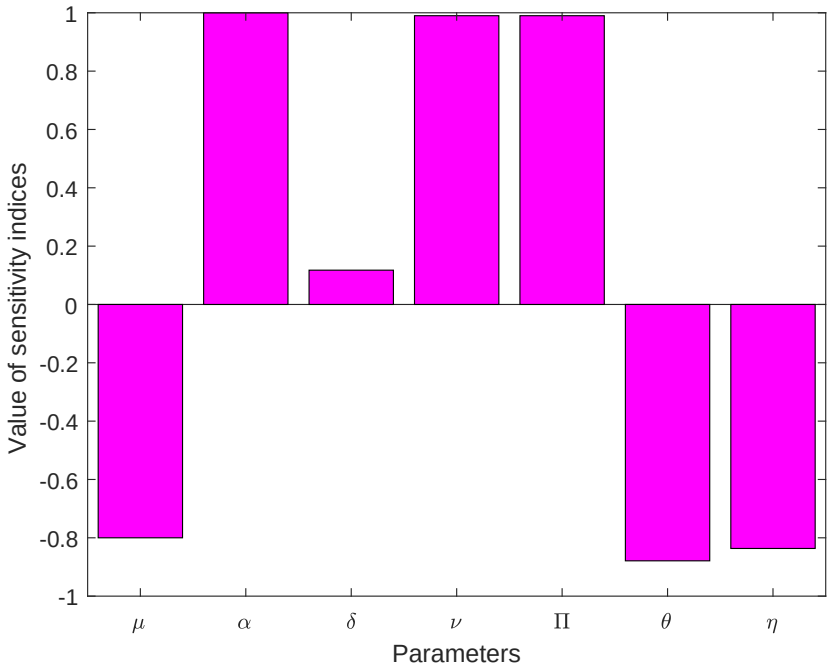

Figure 13. The outcome shows the normalized forward sensitivity indices for the fundamental ratio $\mathcal{R}_0$ with respect to each of the typical variables of the model

Declarations

Use of AI tools

The authors declare that they have not used Artificial Intelligence (AI) tools in the creation of this article.

Data availability statement

Data sharing is not applicable to this article as no datasets were generated or analyzed during the current study.

Ethical approval

The authors state that this research complies with ethical standards. This research does not involve either human participants or animals.

Consent for publication

Not applicable

Conflicts of interest

The authors declare that they have no known competing financial interests or personal relationships that could have appeared to influence the work reported in this paper.

Funding

No funding was obtained for this study.

Author's contributions

S.I.O.: Methodology, Conceptualization, Validation, Software, Data Curation, Writing - Original Draft. M.E.K.: Writing-Review & Editing, Supervision. All authors have read and agreed to the

published version of the manuscript.

Acknowledgements

The authors extend their appreciation to the editor and anonymous reviewers for their thorough review and valuable comments and suggestions, which significantly contributed to enhancing the quality of the paper.

References

[1] World Health Organization (WHO), Coronavirus (COVID-19), Events as They Happen, 31.07.2020. https://www.who.int/emergencies/diseases/novel-coronavirus-2019/events-as-they-happen.

[2] Cavallo, J.J., Donoho, D.A. and Forman, H.P. Hospital capacity and operations in the coronavirus disease 2019 (COVID-19) pandemic—planning for the Nth patient. *JAMA Health Forum*, 1(3), e200345, (2020). [CrossRef]

[3] Ahmed, H.M., Elbarkouky, R.A., Omar, O.A.M. and Ragusa, M.A. Models for COVID-19 daily confirmed cases in different countries. *Mathematics*, 9(6), 659, (2021). [CrossRef]

[4] Alansari, M. and Shagari, M.S. Analysis of fractional differential inclusion models for COVID-19 via fixed point results in metric space. *Journal of Function Spaces*, 2022, 8311587, (2022). [CrossRef]

[5] Mustafa, H.I., Al-shami, T.M. and Wassef, R. Rough set paradigms via containment neighborhoods and ideals. *Filomat*, 37(14), 4683-4702, (2023). [CrossRef]

[6] Kifle, Z.S. and Lemecha Obsu, L. Optimal control analysis of a COVID-19 model. *Applied Mathematics in Science and Engineering*, 31(1), 2173188, (2023). [CrossRef]

[7] Akanni, J.O., Fatmawati and Chukwu, C.W. On the fractional-order modeling of COVID-19 dynamics in a population with limited resources. *Communications in Mathematical Biology and Neuroscience*, 2023, 12, (2023). [CrossRef]

[8] Singh, H., Srivastava, H.M., Hammouch, Z. and Nisar, K.S. Numerical simulation and stability analysis for the fractional-order dynamics of COVID-19. *Results in Physics*, 20, 103722, (2021). [CrossRef]

[9] Chen, Y., Liu, Q. and Guo, D. Emerging coronaviruses: genome structure, replication, and pathogenesis. *Journal of Medical Virology*, 92(4), 418-423, (2020). [CrossRef]

[10] Ouaziz, S.I. and Khomssi, M.E. Dynamics and optimal control methods for the COVID-19 model. IN *Mathematical Modeling and Intelligent Control for Combating Pandemics* (pp. 21-38). Springer Optimization and Its Applications, 203, (2023). [CrossRef]

[11] Uçar, S., Uçar, E., Özdemir, N. and Hammouch, Z. Mathematical analysis and numerical simulation for a smoking model with Atangana–Baleanu derivative. *Chaos, Solitons & Fractals*, 118, 300-306, (2019). [CrossRef]

[12] Makinde, O.D., Akanni, J.O. and Abidemi, A. Modelling the impact of drug abuse on a nation's education sector. *Journal of Applied Nonlinear Dynamics*, 12(1), 53-73, (2023). [CrossRef]

[13] Tang, B., Wang, X., Li, Q., Bragazzi, N.L., Tang, S., Xiao, Y. and Wu, J. Estimation of the transmission risk of the 2019-nCoV and its implication for public health interventions. *Journal of Clinical Medicine*, 9(2), 462, (2020). [CrossRef]

[14] Srivastava, A. and Chowell, G. Understanding spatial heterogeneity of COVID-19 pandemic using shape analysis of growth rate curves. *MedRxiv*, (2020). [CrossRef]

[15] Eikenberry, S.E., Mancuso, M., Iboi, E., Phan, T., Eikenberry, K., Kuang, Y. et al. To mask or not to mask: Modeling the potential for face mask use by the general public to curtail the COVID-19 pandemic. *Infectious Disease Modelling*, 5, 293-308, (2020). [CrossRef]

[16] Okosun, K.O., Rachid, O. and Marcus, N. Optimal control strategies and cost-effectiveness analysis of a malaria model. *BioSystems*, 111(2), 83-101, (2013). [CrossRef]

[17] Ghosh, J.K., Biswas, S.K., Sarkar, S. and Ghosh, U. Mathematical modelling of COVID-19: a case study of Italy. *Mathematics and Computers in Simulation*, 194, 1-18, (2022). [CrossRef]

[18] Johansson, M.A., Quandelacy, T.M., Kada, S., Prasad, P.V., Steele, M., Brooks, J.T. et al. SARS-CoV-2 transmission from people without COVID-19 symptoms. *JAMA Network Open*, 4(1), e2035057, (2021). [CrossRef]

[19] Asamoah, J.K.K., Okyere, E., Abidemi, A., Moore, S.E., Sun, G.Q., Jin, Z. et al. Optimal control and comprehensive cost-effectiveness analysis for COVID-19. *Results in Physics*, 33, 105177 (2022). [CrossRef]

[20] Samui, P., Mondal, J. and Khajanchi, S. A mathematical model for COVID-19 transmission dynamics with a case study of India. *Chaos, Solitons & Fractals*, 140, 110173, (2020). [CrossRef]

[21] Khan, M.A. and Atangana, A. Mathematical modeling and analysis of COVID-19: a study of new variant Omicron. *Physica A: Statistical Mechanics and its Applications*, 599, 127452, (2022). [CrossRef]

[22] Yang, H., Lin, X., Li, J., Zhai, Y. and Wu, J. A review of mathematical models of COVID-19 transmission. *Contemporary Mathematics*, 4(1), 75-98, (2023). [CrossRef]

[23] Capasso, V. and Serio, G. A generalization of the Kermack-McKendrick deterministic epidemic model. *Mathematical Biosciences*, 42(1-2), 43–61, (1978). [CrossRef]

[24] Buonomo, B., d'Onofrio, A. and Lacitignola, D. Global stability of an SIR epidemic model with information dependent vaccination. *Mathematical Biosciences*, 216(1), 9-16, (2008). [CrossRef]

[25] Khajanchi, S., Sarkar, K. and Mondal, J. Dynamics of the COVID-19 pandemic in India. *ArXiv Preprint, ArXiv:2005.06286*, (2020). [CrossRef]

[26] Akanni, J.O., Akinpelu, F.O., Olaniyi, S., Oladipo, A.T. and Ogunsola, A.W. Modelling financial crime population dynamics: optimal control and cost-effectiveness analysis. *International Journal of Dynamics and Control*, 8, 531–544, (2020). [CrossRef]

[27] Diekmann, O., Heesterbeek, J.A.P. and Roberts, M.G. The construction of next-generation matrices for compartmental epidemic models. *Journal of the Royal Society Interface*, 7(47), 873–885, (2010). [CrossRef]

[28] Iggidr, A., Mbang, J., Sallet, G. and Tewa, J.J. Multi-compartment models. *Discrete and Continuous Dynamical Systems Supplement*, 2007, 506-519, (2007). [CrossRef]

[29] Cvetković, A. Stabilizing the Metzler matrices with applications to dynamical systems. *Calcolo*, 57, 1, (2020). [CrossRef]

[30] Korobeinikov, A. and Maini, P.K. A Lyapunov function and global properties for SIR and SEIR epidemiological models with nonlinear incidence. *Mathematical Biosciences & Engineering*, 1(1), 57–60, (2004). [CrossRef]

[31] Chitnis, N., Hyman, J.M. and Cushing, J.M. Determining important parameters in the spread of malaria through the sensitivity analysis of a mathematical model. *Bulletin of Mathematical Biology*, 70, 1272–1296, (2008). [CrossRef]

[32] Berhe, H.W. and Makinde, O.D. Computational modelling and optimal control of measles epidemic in human population. *Biosystems*, 190, 104102, (2020). [CrossRef]

[33] Abidemi, A., Akanni, J.O. and Makinde, O.D. A non-linear mathematical model for analysing the impact of COVID-19 disease on higher education in developing countries. *Healthcare Analytics*, 3, 100193, (2023). [CrossRef]

[34] Gaff, H.D., Schaefer, E. and Lenhart, S. Use of optimal control models to predict treatment time for managing tick-borne disease. *Journal of Biological Dynamics*, 5(5), 517–530, (2011). [CrossRef]

[35] Fleming, W.H. and Rishel, R.W. *Deterministic and Stochastic Optimal Control* (Vol. 1). New York: Springer-Verlag, (1975). [CrossRef]

[36] Coddington, E.A., Levinson, N. and Teichmann, T. Theory of ordinary differential equations. *Physics Today*, 9(2), 18, (1956).

[37] Aseev, S.M. and Kryazhimskii, A.V. The Pontryagin maximum principle and optimal economic growth problems. *Proceedings of the Steklov Institute of Mathematics*, 257, 1–255, (2007). [CrossRef]

[38] World Health Organization (WHO), Coronavirus disease (COVID-19). https://www.who.int/emergencies/diseases/novel-coronavirus-2019.

[39] Kouidere, A., Kada, D., Balatif, O., Rachik, M. and Naim, M. Optimal control approach of a mathematical modeling with multiple delays of the negative impact of delays in applying preventive precautions against the spread of the COVID-19 pandemic with a case study of Brazil and cost-effectiveness. *Chaos, Solitons & Fractals*, 142, 110438, (2021). [CrossRef]

[40] Abidemi, A. and Akanni, J.O. Dynamics of illicit drug use and banditry population with optimal control strategies and cost-effectiveness analysis. *Computational and Applied Mathematics*, 41, 53, (2022). [CrossRef]

[41] Alhassan, A., Momoh, A.A., Abdullahi, A.S. and Kadzai, M.T.Y. Optimal control strategies and cost effectiveness analysis of a malaria transmission model. *Mathematical Theory and Modeling*, 7(6), 123-138, (2017).

[42] Kada, D., Labzai, A., Balatif, O., Rachik, M. and Labriji, E. H. Spread of COVID-19 in Morocco discrete mathematical modeling: optimal control strategies and cost-effectiveness analysis. *Journal of Mathematical and Computational Science*, 10(5), 2070-2093, (2020). [CrossRef]

[43] Marsudi, Hidayat, N. and Wibowo, R.B.E. Optimal control and cost-effectiveness analysis of HIV model with educational campaigns and therapy. *Matematika*, 123-138, (2019).

[44] Dietz, K. The estimation of the basic reproduction number for infectious diseases. *Statistical Methods in Medical Research*, 2(1), 23-41, (1993).
[CrossRef]

How to cite this article: Ouaziz, S.I. & Khomssi, M.E. (2024). Mathematical approaches to controlling COVID-19: optimal control and financial benefits. *Mathematical Modelling and Numerical Simulation with Applications*, 4(1), 1-36. https://doi.org/10.53391/mmnsa.1373093